Frequent downregulation of *LRRC26* by epigenetic alterations is involved in the malignant progression of triple-negative breast cancer

YOSHIMASA MIYAGAWA[1,2*], YOSUKE MATSUSHITA[1*], HIROMU SUZUKI[3], MASATO KOMATSU[1], TETSURO YOSHIMARU[1], RYUICHIRO KIMURA[1], AYAKO YANAI[1,2], JUNKO HONDA[4], AKIRA TANGOKU[5], MITSUNORI SASA[6], YASUO MIYOSHI[2] and TOYOMASA KATAGIRI[1]

[1]Division of Genome Medicine, Institute for Genome Research, Tokushima University, Tokushima 770-8503; [2]Department of Surgery, Division of Breast and Endocrine Surgery, Hyogo College of Medicine, Nishinomiya, Hyogo 663-8501; [3]Department of Molecular Biology, Sapporo Medical University, Sapporo, Hokkaido 060-8556; [4]Department of Surgery, National Hospital Organization Higashitokushima Medical Center, Tokushima 779-0193; [5]Department of Thoracic and Endocrine Surgery and Oncology, Institute of Health Biosciences, The University of Tokushima Graduate School, Tokushima 770-8503; [6]Department of Surgery, Tokushima Breast Care Clinic, Tokushima 770-0052, Japan

Received September 13, 2017; Accepted February 21, 2018

DOI: 10.3892/ijo.2018.4301

Abstract. Triple-negative breast cancer (TNBC), defined as breast cancer lacking estrogen- and progesterone-receptor expression and human epidermal growth factor receptor 2 (HER2) amplification, is a heterogeneous disease. RNA-sequencing analysis of 15 TNBC specimens and The Cancer Genome Atlas-TNBC dataset analysis identified the frequent downregulation of leucine-rich repeat-containing 26 (*LRRC26*), which negatively regulates nuclear factor-κB (NF-κB) signaling, in TNBC tissues. Quantitative polymerase chain reaction and bisulfite pyrosequencing analyses revealed that *LRRC26* was frequently silenced in TNBC tissues and cell lines as a result of promoter methylation. *LRRC26* expression was restored by 5-aza-2'-deoxycytidine (5'-aza-dC) treatment in HCC1937 TNBC cells, which lack *LRRC26* expression. Notably, small interfering RNA-mediated knockdown of *LRRC26* expression significantly enhanced the anchorage-independent growth, invasion and migration of HCC70 cells, whereas ectopic overexpression of *LRRC26* in BT20 cells suppressed their invasion and migration. Conversely, neither knockdown nor overexpression of *LRRC26* had an effect on cell viability in the absence of tumor necrosis factor-α (TNF-α) stimulation. Meanwhile, overexpression of *LRRC26* caused the reduction of TNF-α-mediated NF-κB luciferase reporter activity, whereas depleting *LRRC26* expression resulted in the upregulation of TNF-α-mediated NF-κB downstream genes [interleukin-6 (IL-6), IL-8 and C-X-C motif chemokine ligand-1]. Taken together, these findings demonstrate that *LRRC26* is frequently downregulated in TNBC due to DNA methylation and that it suppresses the TNF-α-independent anchorage-independent growth, invasion and migration of TNBC cells. Loss of *LRRC26* function may be a critical event in the aggressiveness of TNBC cells through a TNF-α/NF-κB-independent mechanism.

Correspondence to: Dr Toyomasa Katagiri, Division of Genome Medicine, Institute for Genome Research, Tokushima University, 3-18-15 Kuramoto-cho, Tokushima 770-8503, Japan
E-mail: tkatagi@genome.tokushima-u.ac.jp

*Contributed equally

Key words: LRRC26, triple-negative breast cancer, tumor suppressor, hypermethylation

Introduction

Triple-negative breast cancer (TNBC), defined as a clinical breast cancer subtype that is negative for estrogen receptor (ER) and progesterone receptor (PgR) expression and human epidermal growth factor receptor 2 (HER2) gene amplification, accounts for 15% of all invasive breast cancer cases. TNBC comprises a heterogeneous group of tumors with different histological and molecular characteristics. Clinically, as TNBC patients do not benefit from endocrine therapies (selective estrogen receptor modulators, selective estrogen receptor downregulators and aromatase inhibitors) (1-3) or anti-HER2 drugs (trastuzumab, lapatinib, pertuzumab and trastuzumab emtansine) (4) due to a lack of targeted therapeutic receptors (5,6), these therapies are not recommended in National Comprehensive Cancer Network guidelines (7). Therefore, chemotherapy using conventional cytotoxic agents, including anthracyclines, cyclophosphamides, taxanes, platinum agents and eribulin (8,9), is currently the mainstay of systemic treatment, although patients with TNBC have worse outcomes following chemotherapy than patients with breast

cancer of other subtypes, including hormone receptor-positive and HER2-positive breast cancer (5,6,10). Thus, since there is no optimized standard chemotherapy protocol for TNBC, detailed subtyping of TNBC is necessary to identify more effective molecular-targeted therapies.

Current omics-based studies, such as genomics and transcriptomics, can provide data that can be used to categorize TNBC. Recent gene expression profiling-based cluster analysis using a dataset consisting of 587 TNBC cases from 21 independent datasets identified six subtypes, including two basal-like subtypes, as well as an immunomodulatory, a mesenchymal, a mesenchymal stem-like and a luminal androgen receptor subtype (11). Moreover, next generation sequencing (NGS)-based studies detected tumor protein p53 and phosphatidylinositol-4,5-bisphosphate 3-kinase catalytic subunit α mutations in 80 and 9% of TNBC cases, respectively (12), highlighting these gene mutations as key genetic events in this subtype. Notably, additional NGS studies led to the identification of actionable molecular characteristics, including 'BRCAness', defined as a defect in homologous recombination repair due to BRCA1 DNA repair associated (BRCA1) or BRCA2 mutation, in TNBC (13,14). Recently, poly(ADP-ribose) polymerase inhibitors were shown to take advantage of synthetic lethality in targeting TNBC with BRCAness (15,16). Furthermore, the nuclear factor-κB (NF-κB) signaling pathway is constitutively activated in the basal-like subtype of breast cancer cells, ~80% of which include TNBC (17). However, the underlying causes of NF-κB signaling activation have remained poorly understood.

To characterize the molecular features of TNBC, RNA-sequencing (RNA-seq) analysis was performed in the present study and it was found that leucine-rich repeat (LRR)-containing 26 (*LRRC26*), a member of the LRR superfamily, was frequently downregulated in patients with TNBC. *LRRC26*, also known as CAPC, is reported to act as a negative regulator of NF-κB activity, and to inhibit cancer cell proliferation and migration (18). However, the pathophysiological role of *LRRC26* in carcinogenesis and TNBC progression, particularly the mechanisms regulating *LRRC26* expression, has not yet been elucidated.

The present study aimed to characterize the molecular mechanism of *LRRC26* downregulation in TNBC.

Materials and methods

Cell lines and clinical specimens. The human breast cancer cell lines, MDA-MB-231, HCC1143, BT-20, BT-549, HCC1395, HCC1937, MDA-MB-157, HCC38, HCC70, MDA-MB-468, BT-474, SK-BR-3, T-47D and ZR-75-1, were purchased from the American Type Culture Collection (Rockville, MD, USA). MCF-7 cells were obtained from the Health Science Research Resources Bank (Osaka, Japan). 293T cells and MDA-MB-453 cells were provided by the RIKEN BioResource Center (Tsukuba, Japan). KPL-3C cells were kindly provided by Dr Junichi Kurebayashi (Kawasaki Medical School, Kurashiki, Okayama, Japan) (19). Each cell line was cultured according to optimal conditions recommended by their respective depositors (Table I). No Mycoplasma contamination was detected in any of the cultures using a Mycoplasma Detection kit (Takara Bio, Inc., Otsu, Japan). A total of 26 TNBC samples and 26 normal mammary tissues were surgically resected with informed consent from patients who were treated at the Tokushima Breast Care Clinic (Tokushima, Japan), as previously described (20) (Table II). Samples were immediately embedded in TissueTek OCT compound (Sakura, Tokyo, Japan), frozen and stored at -80˚C.

The present study, as well as the use of all clinical materials aforementioned, was approved by the Ethics Committee of Tokushima University (Tokushima, Japan).

RNA-seq analysis. Total RNA was extracted from frozen tumors and adjacent normal breast tissues from the 15 out of 26 TNBC samples that could produce a large enough amount of RNA for RNA seq analysis using the Nucleospin RNA II system (Takara Bio, Inc.) according to the manufacturer's protocols. Whole-transcriptome RNAs seq analysis was performed using the SureSelect strand-specific RNA library preparation kit (Agilent Technologies, Inc., Santa Clara, CA, USA) according to the manufacturer's protocols, followed by paired-end 100-bp sequencing on an Illumina HiSeq 1500 platform (Illumina, Inc., San Diego, CA, USA). All primary sequence data files are deposited in the DNA Data Bank of Japan (accession no. JGAS00000000116; http://www.ddbj.nig.ac.jp/). Data were analyzed using CLC Biomedical Genomics Workbench version 4.0 (Qiagen GmbH, Hilden, Germany) with default parameters. Transcript abundance was calculated as transcript per million.

Quantitative PCR (qPCR) and semi-quantitative PCR. Total RNA extracted from clinical breast cancer samples and breast cancer cell lines using the NucleoSpin RNA II system (Takara Bio, Inc.) and the poly A-RNAs of a normal human mammary gland (Clontech Laboratories, Inc., Mountainview, CA, USA) were reverse transcribed using SuperScript II (Life Technologies; Thermo Fisher Scientific, Inc., Waltham, MA, USA). qPCR analysis using the ABI PRISM 7500 Real-Time PCR system was performed with SYBR® Premix Ex Taq (both from Applied Biosystems; Thermo Fisher Scientific, Inc.). The thermocycling conditions were 10 min at 94˚C, followed by 45 cycles of denaturation at 94˚C for 15 sec, 1 min annealing and extension at 60˚C, and reading of the fluorescence. Following threshold-dependent cycling, melting curve analysis was performed from 60 to 94˚C. The quantitative calculation was analyzed using $2^{-\Delta\Delta Cq}$ (21). Semi-quantitative PCR analysis was performed as described previously (22,23). Gene-specific primers used for qPCR and semi-quantitative PCR were as follows: *LRRC26* forward, 5'-CTGCTGCTGGACCACAACC-3' and reverse, 5'-AGAAGGCTCGCACATGCAC-3'; interleukin-6 (*IL-6*) forward, 5'-GGGCATTCCTTCTTCTGG-3' and reverse, 5'-ACTGCATAGCCACTTTCCA-3'; *IL-8* forward, 5'-GCAAAATTGAGGCCAAGG-3' and reverse, 5'-GGCACA GTGGAACAAGGA-3'; and C-X-C motif chemokine ligand-1 (*CXCL-1*) forward, 5'-GCTCTTCCGCTCCTCTCACA-3' and reverse, 5'-GCTTCCTCCTCCCTTCTGGT-3'. The β-actin primer sequences used as quantitative controls were as follows: Forward, 5'-ATTGCCGACAGGATGCAG-3' and reverse, 5'-CTCAGGAGGAGCAATGATCTT-3' for qPCR; and forward, 5'-GAGGTGATAGCATTGCTTTCG-3' and reverse, 5'-CAA GTCAGTGTACAGGTAAGC-3' for semi-quantitative PCR.

Table I. A usage list of the breast cancer cell lines.

Cell line	Temperature (˚C)	Atmosphere	Media + supplements	Analyses performed
MDA-MB-231	37	Air, 100%	Leibovitz's L-15 + 10% FBS with 1% Ab	qPCR, pyrosequencing
HCC1143	37	Air, 95%; CO_2, 5%	RPMI-1640 + 10% FBS with 1% Ab	qPCR, pyrosequencing
BT-20	37	Air, 95%; CO_2, 5%	MEM + 10% FBS with 1% Ab	qPCR, pyrosequencing, bisulfite-sequencing
BT-549	37	Air, 95%; CO_2, 5%	RPMI-1640 + 10% FBS with 1% Ab	qPCR
HCC1395	37	Air, 95%; CO_2, 5%	RPMI-1640 + 10% FBS with 1% Ab	qPCR
HCC1937	37	Air, 95%; CO_2, 5%	RPMI-1640 + 10% FBS with 1% Ab	qPCR, pyrosequencing, bisulfite-sequencing
MDA-MB-157	37	Air, 100%	Leibovitz's L-15 + 10% FBS with 1% Ab	qPCR, pyrosequencing
HCC38	37	Air, 95%; CO_2, 5%	RPMI-1640 + 10% FBS with 1% Ab	qPCR
HCC70	37	Air, 95%; CO_2, 5%	RPMI-1640 + 10% FBS with 1% Ab	qPCR, pyrosequencing, bisulfite-sequencing
MDA-MB-468	37	Air, 100%	Leibovitz's L-15 + 10% FBS with 1% Ab	qPCR
BT-474	37	Air, 95%; CO_2, 5%	MEM + 10% FBS with 1% Ab	qPCR, pyrosequencing
MDA-MB-453	37	Air, 100%	Leibovitz's L-15 + 10% FBS with 1% Ab	qPCR, pyrosequencing
SK-BR3	37	Air, 95%; CO_2, 5%	McCoy's 5a + 10% FBS with 1% Ab	qPCR
T-47D	37	Air, 95%; CO_2, 5%	RPMI-1640 + 10% FBS with 1% Ab	qPCR
ZR-75-1	37	Air, 95%; CO_2, 5%	RPMI-1640 + 10% FBS with 1% Ab	qPCR
KPL-3C	37	Air, 95%; CO_2, 5%	RPMI-1640 + 10% FBS with 1% Ab	qPCR
MCF-7	37	Air, 95%; CO_2, 5%	MEM + 10% FBS with 1% Ab, 0.1 mM NEAA, 1 mM sodium pyruvate and 10 μg/ml insulin	qPCR

RPMI-1640 medium, FBS and insulin were obtained from Sigma-Aldrich; Merck KGaA (Darmstadt, Germany). Leibovitz's L-15, MEM, McCoy's 5a, NEAA and sodium pyruvate were purchased from Thermo Fisher Scientific, Inc. (Waltham, MA, USA). Ab-antimycotic (Thermo Fisher Scientific, Inc.) included penicillin, streptomycin and amphotericin B. FBS, fetal bovine serum; MEM, minimal essential medium; NEAA, Non-Essential Amino Acids; Ab, antibody; qPCR, quantitative polymerase chain reaction.

Methylation analysis using bisulfite pyrosequencing and bisulfite sequencing. Genomic DNA (1 μg) extracted from clinical samples and cell lines was modified with sodium bisulfite using an EpiTect Bisulfite kit (Qiagen GmbH), subsequent to which bisulfite pyrosequencing was performed as previously described (24). The methylation ratio (%) of *LRRC26* in each sample was analyzed using PyroMark Q96 software version 2.5.8 (Qiagen GmbH). For bisulfite sequencing, thermocycling conditions were 10 min at 94˚C, followed by 45 cycles of denaturation at 94˚C for 1 min, annealing at 60˚C for 1 min and extension at 72˚C for 10 min. Amplified PCR products were cloned into the pCR2.1-TOPO vector (Thermo Fisher Scientific, Inc.), and 11 clones from HCC1937, 12 clones from BT-20 and 15 clones from HCC70 were sequenced using an ABI3130x automated sequencer (Thermo Fisher Scientific, Inc.). Primer sequences and PCR product sizes are listed in Table III.

5'-aza-dC treatment. To restore epigenetically silenced *LRRC26* gene expression, HCC1937 cells were plated onto 6-well dishes at a density of $3.5x10^5$ cells/well and treated with several concentrations (0, 1, 2.5, 5 and 10 μM) of 5'-aza-dC (Sigma-Aldrich; Merck KGaA, Darmstadt, Germany) for 5 days, replacing the reagent and RPMI-1640 (Sigma-Aldrich; Merck KGaA) medium every 24 h. *LRRC26* gene expression following treatment with 5'-aza-dC was monitored by semi-quantitative PCR as aforementioned.

Small interfering RNA (siRNA)-mediated gene silencing. ON-TARGETplus siRNA-SMARTpool (4 types of siRNA; catalog no. L-029447-01-0005; GE Healthcare Dharmacon, Inc., Lafayette, CO, USA) was used to knockdown *LRRC26* expression in the HCC70 cells, with siRNA against enhanced green fluorescent protein (si-EGFP) used as a control. HCC70 cells were plated in 6-well dishes at $1.0x10^5$ cells/well. Transfection of 10 nM ON-TARGETplus siRNAs was performed using Lipofectamine RNAiMax (Thermo Fisher Scientific, Inc.) according to the manufacturer's protocols. Knockdown efficiency was evaluated by qPCR using the aforementioned protocol at 48, 72, 96 and 120 h post-transfection. Cell proliferation assays were performed using Cell Counting Kit-8 (Dojindo Molecular Technologies, Inc., Kumamoto, Japan) as previously described (20). All experiments were performed in triplicate.

Soft agar colony formation assay. Anchorage-independent growth was assessed by the soft agar assay. HCC70 cells were transfected with 10 nM ON-TARGETplus siRNAs for 36 h,

Table II. Clinical and pathological features of 26 triple-negative breast cancer cases enrolled in RNA-seq and qPCR analyses.

Case_ID	Age (years)	Gender	ER	PgR	HER2	Histology	T-stage	Node
10	57	F	(-)	(-)	1^+	Papillotubular > scirrhous	T2	+
19[a]	44	F	(-)	(-)	0	Papillotubular	T1	-
36	50	F	(-)	(-)	0	Solid-tubular > papillotubular	T2	+
53[a]	55	F	(-)	(-)	0	Papillotubular > scirrhous	T1	-
54[a]	77	F	(-)	(-)	0	Solid-tubular	T1	-
56[a]	58	F	(-)	(-)	0	Solid-tubular	T1	+
101	60	F	(-)	(-)	0	Scirrhous > solid-tubular	T2	+
110[a]	77	F	(-)	(-)	1^+	Scirrhous > papillotubular	T2	+
114[a]	76	F	(-)	(-)	0	Solid-tubular	T2	+
133	50	F	(-)	(-)	0	Solid-tubular	T1	-
150[a]	58	F	(-)	(-)	0	Papillotubular	T2	-
159[a]	75	F	(-)	(-)	1^+	Papillotubular	T1	-
171	37	F	(-)	(-)	1^+	Solid-tubular	T1	+
179[a]	61	F	(-)	(-)	0	Solid-tubular	T2	-
188	50	F	(-)	(-)	1^+	Solid-tubular > scirrhous	T1	-
192[a]	50	F	(-)	(-)	0	Solid-tubular	T1	+
209[a]	50	F	(-)	(-)	0	Solid-tubular > scirrhous	T2	+
242	58	F	(-)	(-)	0	Unknown (large cell)	T3	+
270[a]	47	F	<5	<5	0	Solid-tubular	T1	-
272[a]	88	F	<5	<5	0	Solid-tubular	T2	-
284[a]	58	F	(-)	(-)	0	Papillotubular	T2	+
292[a]	69	F	<5	<5	0	Solid-tubular > scirrhous	T2	+
306	83	F	<5	<5	1^+	Invasive lobular	T2	-
320	70	F	(-)	(-)	0	Scirrhous > papillotubular	T1	-
329	32	F	<5	<5	0	Papillotubular	T1	-
334	63	F	<5	<5	0	Adenoid cystic	T1	-

All cases were analyzed by qPCR. [a]Cases which also underwent RNA-Seq. The evaluation of HER2 protein expression was performed by immunohistochemistry assay of the invasive component of a breast cancer specimen (41). TNM classification was classified by General Rules for Clinical and Pathological Recording of Breast Cancer edited by the Japanese Breast Cancer Society that referred to the International Union Against Cancer (42). qPCR, quantitative polymerase chain reaction; RNA-Seq, RNA sequencing; ER, estrogen receptor; PgR, progesterone receptor; HER2, human epidermal growth factor receptor 2; F, female.

Table III. Primer sequences used for bisulfite pyrosequencing and bisulfite sequencing of *LRRC26*.

Primer	Primer sequences	Size (bp)
Bisulfite pyrosequence		
Forward primer (Seq.1-2)	TGGGCGGTGTTTTGTTGTTTAGGTTA	119
Reverse primer (Seq.1-2)	Bio_AAAACTCCAAACTACTCTTAACTCAAC	
Forward primer (Seq.TCGA)	AGGTTTTATTTAGTATGGGAATGGGATT	123
Reverse primer (Seq.TCGA)	Bio_AACCCAAAAATCCTACTCCTCACCC	
Sequencing primer (Seq.1)	TTGTTTAGGTTAGGGTT	
Sequencing primer (Seq.2)	GAGGTGGTTTTGATAG	
Sequencing primer (Seq.TCGA)	GGAATGGGATTATTTTTG	
Sequence to analyze (Seq.1)	CGGCGGGCG	
Sequence to analyze (Seq.2)	CGTTGTGGTCGGCG	
Sequence to analyze (Seq.TCGA)	CGTGGGGGTTATTTCGTATGTGTACG	
Bisulfite sequence		
Forward primer (Seq.1-2)	TGGGCGGTGTTTTGTTGTTTAGGTTA	343
Reverse primer	AACCCCGCATAAAAACAACCCCCC	

Reverse primers of bisulfite pyrosequence are 5'-biotinylated. Underlining indicates a possible CpG site of LRRC26. LRRC26, leucine-rich repeat-containing 26.

and 2.5x10^3 cells were plated in triplicate in 5 ml RPMI-1640 medium containing 0.4% soft agarose, overlaid on 5 ml 0.72% agarose in 6-cm dishes and cultured at 37˚C for 11 days. Colonies per well were counted on a Power IX71 microscope (Olympus Corporation, Tokyo, Japan).

Migration assay. BD Falcon Cell Culture Inserts (24 wells, 8-μm pore size; BD Biosciences, Franklin Lakes, NJ, USA) were rehydrated with serum-free RPMI-1640 at 37˚C in a 5% CO_2 incubator for 2 h. Following rehydration, the medium was removed and 0.5 ml RPMI-1640 was added to the upper chamber, and 0.5 ml RPMI-1640 with 10% fetal bovine serum (FBS) was added to the lower chamber. RPMI/FBS medium (0.5 ml) containing 2.5x10^4 HCC70 cells previously transfected with siRNA for 36 h was added to each insert. The HCC70 cells in the migration chamber underwent incubation at 37˚C for 48 h. Following incubation, the chamber inserts were fixed (4% paraformaldehyde for 10 min) prior to being stained with 1% Giemsa at room temperature for 2 days. The total number of migrated cells for each treatment was calculated from five random fields for each insert counted on a Power IX71 microscope (Olympus Corporation) at x40 magnification. The number of migrated cells per well for each treatment was averaged from duplicate samples and expressed as the mean ± standard deviation.

Invasion assay. Matrigel invasion chambers (24 wells, 8-μm pore size; Corning Inc., Corning, NY, USA) were rehydrated with serum-free RPMI at 37˚C in a 5% CO_2 incubator for 2 h. Following rehydration, the medium was removed and 0.5 ml RPMI-1640 was added to the upper chamber, and 0.5 ml RPMI-1640 plus 10% FBS was added to the lower chamber. RPMI/FBS medium (0.5 ml) containing 2.5x10^4 HCC70 cells previously transfected with siRNA for 36 h was added to each insert. The HCC70 cells in the invasion chamber were incubated at 37˚C for 48 h. Following incubation, chamber inserts were fixed with 4% paraformaldehyde for 10 min prior to being stained with 1% Giemsa at room temperature for 2 days. The total number of migrated cells for each treatment was calculated from five random fields for each insert counted on a Power IX71 microscope (Olympus Corporation) at x40 magnification. The number of invaded cells per well for each treatment was averaged from duplicate samples and expressed as the mean ± standard deviation.

Construction of expression vectors. pCAGGSSnHC and pCAGGSn3FC, in which an HA-tag and a 3xFLAG-tag, respectively, are inserted in the C-terminus of the cloning sites of pCAGGS vector, were constructed and gifted by Dr Yusuke Nakamura (University of Tokyo, Tokyo, Japan). Briefly, to construct the *LRRC26* and B cell receptor associated protein 31 (*BAP31*) expression vectors, the entire coding sequences of *LRRC26* and *BAP31* cDNAs were amplified by PCR using KOD-Plus DNA polymerase (Toyobo, Osaka, Japan) with the following primers: *LRRC26* forward, 5'-G**GAATTC**ATGCGGGGCCCTTCCTGGTCG-3' and reverse, 5'-CCG**CTCGAG**GGCTTGGGCGGCAGCGGCGG-3'; and BAP31 forward, 5'-CG**GAATTC**ACCATGGGTGCCGAGGCGTCCTC-3' and reverse, 5'-CCG**CTCGAG**CTCTTCCTTCTTGTCCATGGGAC-3' (bold indicates the restriction enzyme sites). The thermocycling conditions were as follows: For *LRRC26*, an initial denaturation of 2 min at 94˚C, followed by 35 cycles of denaturation at 94˚C for 15 sec, annealing at 62˚C for 30 sec and elongation at 68˚C for 80 sec; for BAP31, an initial denaturation of 2 min at 94˚C, followed by 30 cycles of denaturation at 94˚C for 15 sec, annealing at 52˚C for 30 sec and elongation at 68˚C for 1 min. BAP31 is an a transmembrane protein associated with the endoplasmic reticulum (ER) and ER-Golgi intermediates, and has been involved in apoptosis and protein trafficking (25,26). Each PCR product was inserted into the *Eco*RI and *Xho*I sites of pCAGGSnHA in frame with the C-terminal HA-tag (pCAGGSSnHC-*LRRC26*) and pCAGGSn3FC in frame with the C-terminal FLAG-tag (pCAGGSSn3FC-*BAP31*), respectively. To construct the pGL3-NF-κB expression vector for the luciferase reporter assay as described next, the oligonucleotides for NF-κB-U (5'-**C**TGGGGACTTTCCGCTGGGGACTTTCCGCTGGGGACTTTCCGCTGGGGACTTTCCGCTATATA**C**-3') and NF-κB-L (5'-**TCGAG**TATATAGCGGAAAGTCCCCAGCGGAAAGTCCCCAGCGGAAAGTCCCCAGCGGAAAGTCCCCA**GGTAC**-3') (bold font indicates restriction enzyme sites and underlining indicates 4x NF-κB binding sites) was annealed, and cloned into the *Kpn*I and *Xho*I sites of pGL3-basic (Promega Corporation, Madison, WI, USA). The DNA sequence of all constructs were confirmed by DNA sequencing (ABI3500xL; Thermo Fisher Scientific, Inc.).

Luciferase reporter assay. 293T cells (2.0x10^5 cells/well in 6-well plates) were co-transfected with 200 ng pGL3-NF-κB in combination with 1.0 μg pCAGGSnHC-*LRRC26* or the mock vector using Fugene 6 (Promega Corporation). pRL-TK (Promega Corporation) was used as an internal control. After 24 h, the cells were treated with TNF-α (40 ng/ml; Sigma-Aldrich; Merck KGaA) for 0, 4, 8 and 12 h. Next, the cells were harvested and analyzed for Firefly luciferase and *Renilla* luciferase activity using the PicaGene Dual Sea Pansy Luminescence kit (Wako Pure Chemical Industries, Ltd., Osaka, Japan) according to the manufacturer's protocols. Data are expressed as the fold increase over mock-transfected cells (set at 1.0) and represented as the mean ± standard error of two independent experiments.

Analysis of public database of RNA expression and methylation in breast cancer. Publicly available gene expression and methylation data from The Cancer Genome Atlas (TCGA; http://cancergenome.nih.gov/) were downloaded. Differential expression (by fold-change value) between breast cancer and the adjacent normal breast tissues was calculated according to the normalized gene expression value of each sample.

Microarray analysis. HCC70 cells were seeded at a density of 2x10^5 cells/well onto 6-well plates, followed by transfection with 10 nM siEGFP (Sigma-Aldrich; Merck KGaA) or siLRRC26 (GE Heathcare Dharmacon, Inc.) using Lipofectamine RNAiMAX (Thermo Fisher Scientific, Inc.) according to the manufacturer's protocols. After 48 and 72 h of siRNA transfection, total RNA was extracted using a NucleoSpin RNA kit (Takara Bio, Inc.) according to the manufacturer's protocols. A total of 100 ng total RNA from each sample was amplified and Cy3-labeled. Next, 0.825 μg Cy3-labeled cRNA was fragmented, hybridized onto the

Agilent SurePrint G3 Hmn GE 8x60K Ver 2.0 platform (Agilent Technologies, Inc.) and then incubated with rotation at 65˚C for 17 h. Data were analyzed using GeneSpring software version 13.0 (Agilent Technologies, Inc.) as previously described (20). To identify genes that were significantly altered between siLRRC26-treated cells and siEGFP-treated cells, the mean signal intensity values in each analysis were compared. The extent and direction of the differential expression between 48 and 72 h were determined by calculating the fold-change value. Data from this microarray analysis have been submitted to the NCBI Gene Expression Omnibus archive as series GSE90582.

Functional gene annotation clustering. The Database for Annotation, Visualization and Integrated Discovery (DAVID 6.8) was approved to detect functional gene annotation clusters based on gene expression profiling by gene annotation enrichment analysis (http://david.abcc.ncifcrf.gov/) (27,28). The clusters from the gene annotation enrichment analysis were selected in this study based on a previous study (29).

Scratch wound cell migration and invasion assays by IncuCyte. BT20 cells ($2.0x10^5$ cells/well in 6-well plates) were transfected with 2.0 μg pCAGGSnHC-*LRRC26* or the mock vector. For migration assay, after 48 h, cells ($2.5x10^4$ cells/well) were re-seeded onto the 96-well ImageLock™ plate (Essen BioScience, Ann Arbor, MI, USA), which was coated with Matrigel (100 μg/ml) prior to seeding the cells. After 4 h, the wound area was created in the cell monolayer with a 96-well WoundMaker™ (Essen BioScience). The plate was washed with phosphate-buffered saline (PBS) (-) to remove detached cells, and 100 μl fresh medium was added. For the invasion assay, the cells were covered with 50 μl Matrigel solution (8 mg/ml) and incubated for 30 min. Next, 100 μl of additional culture media was added to each well and the plates were placed into the IncuCyte ZOOM (Essen Bioscience). The two plate types were scanned every 2 h for 72 h. Data were analyzed using ZOOM software version 2016B (Essen BioScience) according to the manufacturer's protocols. Cell migration and invasion were expressed as relative wound density.

Immunocytochemical staining analysis. To examine the subcellular localization of the *LRRC26* protein in TNBC cells, BT20 cells ($2.0x10^5$ cells/well in 6-well plates) were transfected with 2.0 μg pCAGGSnHC-*LRRC26* or the mock vector using FuGENE HD transfection regent (Roche Diagnostics GmbH, Mannheim, Germany). In addition, BT-20 cells were co-transfected with 2.0 μg pCAGGSnHC-*LRRC26* and pCAGGSn3FC-*BAP31* or the empty vector (Mock). At 48 h post-transfection, BT-20 cells ($2.0x10^4$ cells/well) were plated onto an 8-well glass slide chamber (Thermo Fisher Scientific, Inc.). After 24 h of incubation, the cells were fixed with 4% paraformaldehyde for 30 min at 4˚C and then peameabilized with 0.1% Triton X-100 for 2 min at room temperature. Next, the cells were covered with 3% bovine serum albumin for 1 h at room temperature and then incubated with anti-HA antibody (1:1,000 dilution; cat. no. 1867423; Roche Diagnostics GmbH) and anti-FLAG M2 (1:1,000 dilution; cat. no. F-3165; Sigma-Aldrich; Merck KGaA) or anti-78-kDa glucose-regulated protein (GRP78; 1:200 dilution; cat. no. ab108615; Abcam, Cambridge, UK) antibodies overnight at 4˚C. Subsequent to washing with PBS (-), the cells were stained with Alexa 488-conjugated anti-rat (cat. no. A-21210) and Alexa 594-conjugated anti-mouse (cat. no. A-11032) or anti-rabbit (cat. no. A-11037) antibodies (1:1,000 dilution; Molecular Probes; Thermo Fisher Scientific, Inc.) at room temperature for 1 h, respectively. The nuclei were stained with 4',6'-diamidine-2'-phenylindole dihydrochloride. Fluorescence was observed was obtained using an IX71 microscope (Olympus Corporation). Scale bars indicate 20 μm.

Immunoblotting analyses. Immunoblotting analyses were conducted as previously described (30). Briefly, cell lysates were prepared with lysis buffer at 48 h post-transfection. The lysates were electrophoresed, transferred to a nitrocellulose membrane and blocked with 4% BlockAce solution (Dainippon Sumimoto Pharma Co., Ltd., Osaka, Japan) for 1 h. Subsequently, the membrane were incubated with anti-HA (1:3,000 dilution; cat. no. 1867423) and anti-α/β-Tubulin antibodies (1:1,000 dilution; cat. no. 2148) (Cell Signaling Technology, Inc., Danvers, MA, USA) at 4˚C overnight, respectively. Following incubation with a horseradish peroxidase-conjugated secondary antibody (1:5,000 dilution; catalog no. sc-2006 for anti-rat antibody; catalog no. sc-2004 for anti-rabbit antibody; Santa Cruz Biotechnology, Inc., Dallas, TX, USA) at room temperature for 1 h, the membranes were developed with an enhanced chemiluminescence system (GE Healthcare Life Sciences, Little Chalfont, UK) and were scanned using an Image Reader LAS-3000 mini (Fujifilm, Tokyo, Japan).

Statistical analysis. Statistical significance was calculated using the Kruskal-Wallis test and Dunnett's post-hoc test with SPSS version 20.0 software (IBM, Armonk, NY, USA) for the comparison between the gene expression and methylation levels from the TCGA dataset. For multiple comparisons of Figs. 1D and 2B, a one-way analysis of variance with Dunnett's and Tukey's post hoc tests, respectively, were performed. Wilcoxon signed rank test was performed using JMP 12.1.0 (SAS Institute Japan, Ltd., Tokyo, Japan) to assess methylation levels between tumor and paired normal tissues. The χ^2 test was performed using Microsoft® Excel 2016 to assess the associations between the expression of the *LRRC26* gene and patient characteristics. Student's two-sided t-test was performed using Microsoft® Excel 2016 to calculate statistical significance in experiments for the gene expression, methylation status, colony formation, migration, invasion and luciferase activity. $P<0.05$ was considered to indicate a statistically significant difference.

Results

LRRC26 is specifically downregulated in TNBC clinical specimens and cell lines due to methylation of CpG islands. To characterize the molecular features of TNBC, RNA-seq analysis was first performed and it was found that *LRRC26* expression was downregulated in 10 out of 15 patients with TNBC, but upregulated in 4 (no regulation change in 1 patient) (Fig. 1A). Subsequent qPCR confirmed that *LRRC26* was significantly downregulated in 16 out of the 26 patients with TNBC (6 of the 15 patients who also underwent RNA-Seq)

Table IV. Association between leucine-rich repeat-containing 26 downregulation in triple-negative breast cancer cases and patient characteristics.

Characteristic	Total	Expression of *LRRC26* for tumor/normal tissue <1.0	Expression of *LRRC26* for tumor/normal tissue ≥1.0	P-value (χ^2 test)
Total, n	26	17 (65.4)	9 (34.6)	
Age in years, n (%)				0.482
≥50	22 (84.6)	15 (57.7)	7 (26.9)	
<50	4 (15.4)	2 (7.7)	2 (7.7)	
Menopause, n (%)				0.743
Post	16 (61.5)	10 (38.5)	6 (23.0)	
Pre	8 (30.8)	6 (23.1)	2 (7.7)	
N/A	2 (7.7)	1 (3.85)	1 (3.85)	
Histological grade, n (%)				0.017
1	7 (26.9)	2 (7.7)	5 (19.2)	
≥2	19 (73.1)	15 (57.7)	4 (15.4)	
T, n (%)				0.216
1	13 (50.0)	7 (27.0)	6 (23.0)	
≥2	13 (50.0)	10 (38.5)	3 (11.5)	
N, n (%)				0.340
-	14 (53.9)	8 (30.8)	6 (23.1)	
+	12 (46.1)	9 (34.6)	3 (11.5)	
M, n (%)				N/A
0	26 (100.0)	17 (65.4)	9 (34.6)	
1	0.0	0.0	0.0	

TNM classification was judged according to the General Rules for Clinical and Pathological Recording of Breast Cancer (the Japanese Breast Cancer Society) that referred to the International Union Against Cancer (42). T, tumor stage; N, lymph node metastasis status; M, distant metastasis.

compared with that in paired normal breast tissues (Fig. 1B), which was consistent with the RNA-seq results. Subsequently, statistical analysis of the association between *LRRC26* expression level and clinicopathological features, including the tumor stage or grade of TNBC cases used for qPCR, was performed, and it was found that *LRRC26* downregulation was significantly associated with increased histological grade in patients with TNBC (P=0.017; χ^2 test) (Table IV). Furthermore, the expression of the *LRRC26* gene was examined by the analysis of TCGA dataset, including a much larger number of TNBC cases and normal controls, and it was found that the *LRRC26* gene was significantly downregulated in 123 TNBC cases compared with that in 113 normal controls (Fig. 1C). These results suggested the possibility that the downregulation of *LRRC26* may be associated with the carcinogenesis of TNBC. Accordingly, the present study focused on understanding the mechanism of *LRRC26* downregulation in TNBC, although further analysis of the mechanism of *LRRC26* upregulation in breast cancer will be necessary. Next, to determine whether *LRRC26* downregulation is associated with CpG hypermethylation in its promoter region, bisulfite pyrosequencing analysis was performed using a set of 12 TNBC clinical tissues and adjacent normal breast tissues. *LRRC26* methylation levels were quantitatively measured at two CpG islands containing 'Seq.1' and 'Seq.2', located 206 and 158 bp upstream of the transcription start site, respectively (Fig. 1D). The average methylation levels of 'Seq.1' in the tumor and normal tissues was 43.63% (range, 18.37-62.89%) and 26.55% (range, 18.47-40.09%), respectively, and that of 'Seq.2' in the tumor and normal tissues was 18.79% (range, 8.52-23.15%) and 11.63% (range, 8.86-15.32%), respectively (Fig. 1D). Accordingly, the methylation levels of the two CpG islands were significantly higher in 11 out of 12 tumor tissues compared with those in adjacent normal mammary gland tissues (Fig. 1D; Wilcoxon signed-rank test: Seq.1, P=0.0015 and Seq.2, P=0.0024, respectively) (Fig. 1D). To further validate this result, *LRRC26* expression levels were analyzed in breast cancer cell lines by qPCR. *LRRC26* expression was significantly downregulated in 8 out of 10 TNBC cell lines compared with that in normal mammary glands (Fig. 1E), whereas its expression level was extremely high in all HER2-positive and ER-positive/HER2-negative cell lines (Fig. 1E). Furthermore, *LRRC26* methylation status was analyzed in TNBC cell lines, and it was observed that high levels of methylation at the two CpG island sites in *LRRC26* were in agreement with *LRRC26* expression levels in 4 out of 6 TNBC cell lines (Fig. 1E and F). Low levels of methylation at the two CpG island sites were in agreement with high levels of *LRRC26* expression in the two HER2-positive cell lines, BT-474 and MDA-MB453. Of the remaining TNBC cell lines, *LRRC26* was expressed in

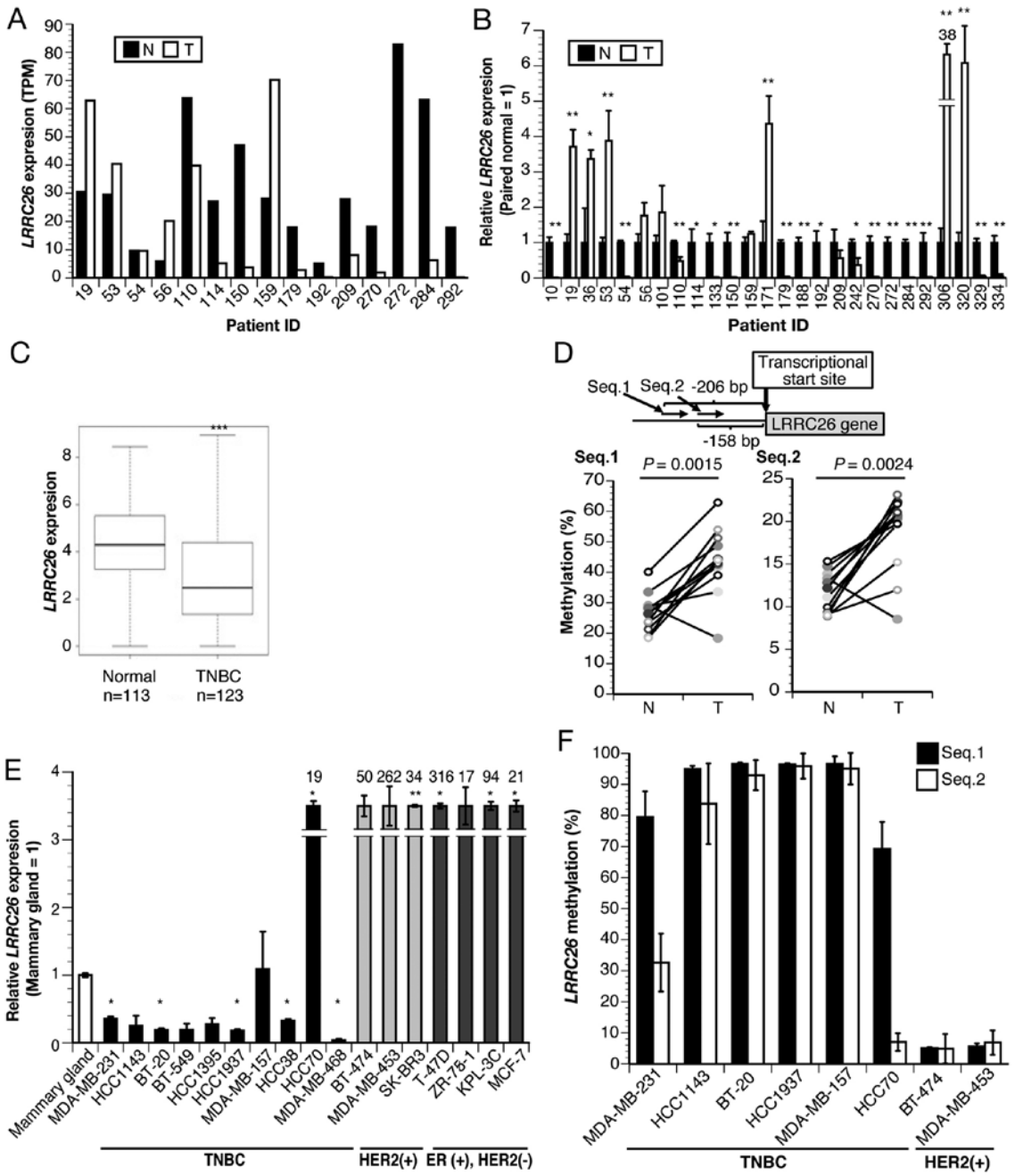

Figure 1. *LRRC26* expression and methylation in TNBC. (A) *LRRC26* expression determined by RNA-seq analysis of 15 TNBC cases. (B) Relative *LRRC26* gene expression in 26 TNBC clinical specimens and paired normal tissues by qPCR. The data represent the mean ± standard deviation of each condition (*P<0.05 and **P<0.01; two-sided Student's t-test). (C) Expression levels in 123 TNBC patients and 113 normal tissues obtained from TCGA RNA-seq datasets. The box plot shows the expression level between TNBC and normal tissue. Two-sided Student's t-test revealed a significant difference (***P<0.001 vs. normal tissues). (D) Diagram of the CpG sites of the *LRRC26* gene. The two regions (Seq.1 and Seq.2) analyzed using bisulfite pyrosequencing are shown (upper panel). Bisulfite pyrosequencing analysis of two *LRRC26* CpG sites (Seq.1 and Seq.2) in 12 TNBC clinical specimens and paired normal breast tissues (lower panel) (Wilcoxon signed-rank test). (E) Relative expression of *LRRC26* gene in 17 breast cancer cell lines, including 10 TNBC, 3 HER2(+) and 4 ER(+) HER2(-) cell lines, compared with that in normal mammary glands, as determined by qPCR. The data represent the mean ± standard deviation of each condition (*P<0.05 and **P<0.01; analysis of variance with Dunnett's post hoc test). (F) Bisulfite pyrosequencing analysis of 2 *LRRC26* CpG sites (Seq.1 and Seq.2) in indicated breast cancer cell lines. The data represent the mean ± standard deviation of each condition. TNBC, triple-negative breast cancer; TPM, transcript per million; *LRRC26*, leucine-rich repeat-containing 26; RNA-seq, RNA sequencing; T, clinical tumor specimens; N, normal tissue; ER, estrogen receptor; HER2, human epidermal growth factor receptor 2; qPCR, quantitative polymerase chain reaction.

HCC70, whereas high DNA methylation levels (>60%) were detected at Seq.1 and low levels at Seq.2. Conversely, *LRRC26* was downregulated in MDA-MB-231, which displayed high DNA methylation levels at Seq.1 and moderate levels at Seq.2 (Fig. 1E and F). These results indicated that a different mechanism, such as histone modification or the existence of other critical CpG sites in the *LRRC26* promoter region, may underlie *LRRC26* silencing in these cells.

LRRC26 downregulation and hypermethylation occur exclusively in TNBC. To clarify the detailed methylation status, bisulfite sequencing was performed using TNBC cell lines

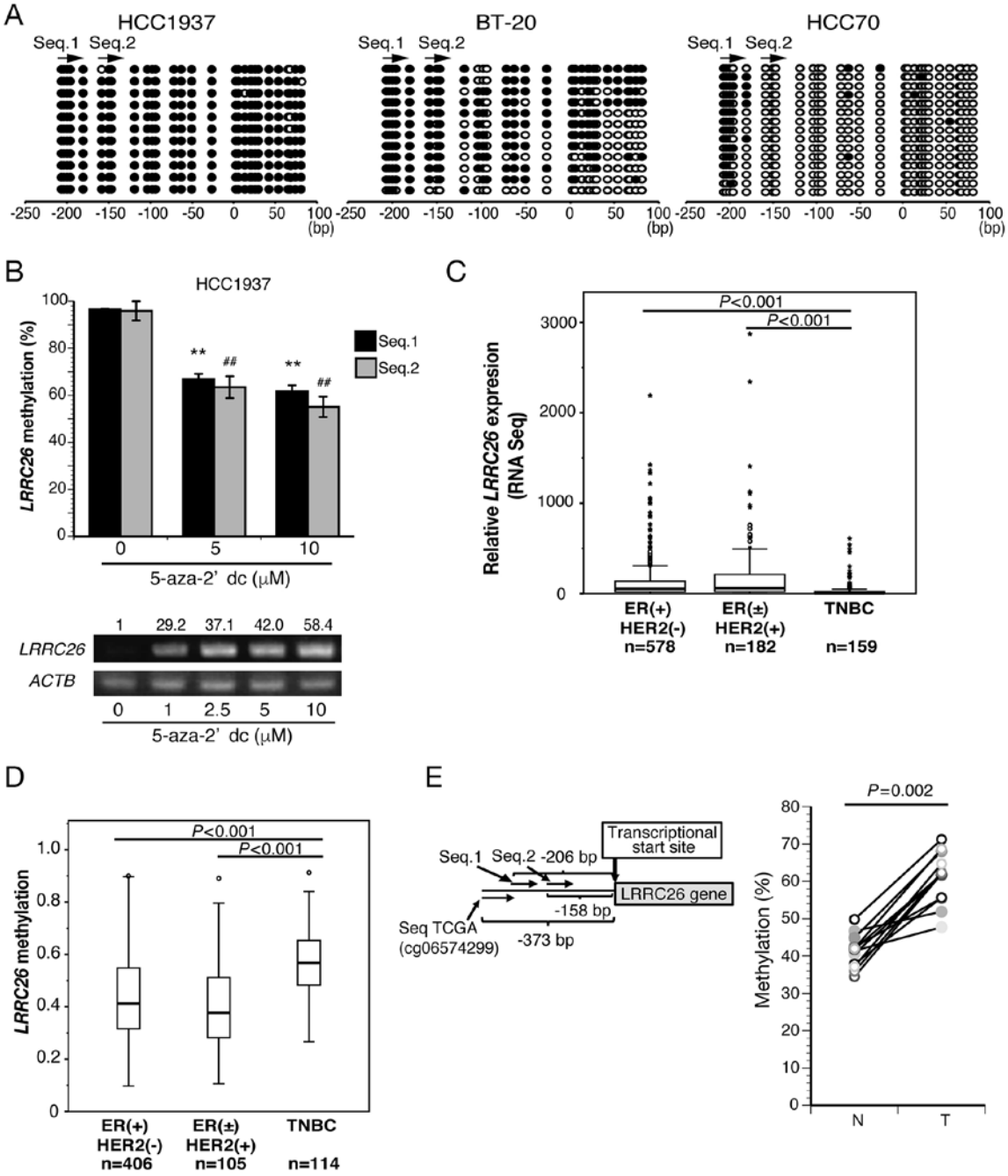

Figure 2. *LRRC26* downregulation and hypermethylation are exclusive to TNBC. (A) Bisulfite sequencing analysis of two *LRRC26* CpG sites in HCC1937, BT20 and HCC70 cells. Open and filled circles represent unmethylated and methylated CpG sites, respectively. The arrow indicates the region analyzed via bisulfite pyrosequencing. (B) Bisulfite pyrosequencing (bar graph) and semi-quantitative PCR results (bottom panel) for *LRRC26* in HCC1937 cells treated with varying doses of 5'-aza-dC for 120 h. Mean methylation levels (%) of *LRRC26* were measured as aforementioned. The data represent the mean ± standard deviation of methylation levels of each CpG island. (**P<0.01 vs. 5'-aza-dC (0 μM) in Seq.1; $^{\#\#}$P<0.01 vs. 5'-aza-dC (0 μM) in Seq.2; analysis of variance with Tukey's post hoc test). (C) *LRRC26* gene expression in 3 subtypes [ER(+)HER2(-), ER(±)HER2(+) and TNBC) for cases with TCGA RNA-seq datasets. The Kruskal-Wallis test revealed a significant difference, followed by Dunnett's post hoc test. (D) Methylation levels in 625 breast cancer patients obtained from TCGA datasets. The box plot shows the percent methylation between three breast cancer subtypes classified by ER status and HER2 expression. The Kruskal-Wallis test revealed a significant difference, followed by Dunnett's post hoc test. (E) Bisulfite pyrosequencing analysis at CpG island SeqTCGA (the CpG island located 373 bp upstream of the transcription start site) in 12 TNBC clinical specimens and paired normal breast tissues (righ panel) (Wilcoxon signed-rank test). The CpG island SeqTCGA site in the *LRRC26* gene is also shown (left panel) (Wilcoxon signed-rank test). 5'-aza-dC, 5-aza-2'-deoxycytidine; TNBC, triple-negative breast cancer; *LRRC26*, leucine-rich repeat-containing 26; *ACTB*, β-actin; RNA-seq, RNA sequencing; ER, estrogen receptor; HER2, human epidermal growth factor receptor 2; T, clinical tumor specimens; N, normal tissue; qPCR, quantitative polymerase chain reaction.

HCC1937, BT20 and HCC70. It was found that the 200 bp upstream of the transcription initiation site, including Seq.1 and Seq.2 CpG islands, in *LRRC26* were densely methylated in HCC1937, but not in HCC70, although the Seq.1 CpG island was methylated (Fig. 2A). Moreover, the same regions in *LRRC26* were partially methylated in BT20, indicating that the methylation levels at the *LRRC26* promoter region were in agreement with the level of *LRRC26* expression in all

three cell lines. Notably, *LRRC26* expression was restored in a dose-dependent manner following treatment with 5'-aza-dC in HCC1937 (Fig. 2B). Moreover, the methylation level of *LRRC26* was also significantly reduced in HCC1937 cells following treatment with 5'-aza-dC (Fig. 2B).

Subsequently, RNA-seq analysis of 919 breast cancer cases from TCGA dataset revealed that *LRRC26* gene expression in TNBC cases was significantly lower than that in other subtypes, such as ER(+)/HER2(-), ER(±)/HER2(+) (Fig. 2C), whereas *LRRC26* gene methylation analysis of 625 cases on the same dataset was significantly higher in TNBC cases than in other subtypes (Fig. 2D). Furthermore, bisulfite pyrosequencing analysis was performed using a set of 12 TNBC clinical tissues and adjacent normal breast tissues to analyze the methylation level of *LRRC26* at seqTCGA located 373 bp upstream of the transcriptional start site (Fig. 2E). The results showed that the methylation level of the seqTCGA CpG island was significantly higher in all tumor tissues than that in the adjacent normal mammary gland tissues (Wilcoxon signed-rank test: P=0.002) (Fig. 2E). These data strongly suggested that low *LRRC26* expression due to hypermethylation in its promoter region is exclusive to TNBC cases.

LRRC26 as a tumor suppressor in TNBC cells. To investigate the impact of *LRRC26* on cell growth in HCC70 TNBC cells, standard cell proliferation assays were performed. First, the knockdown of *LRRC26* expression was confirmed in HCC70 cells, in which *LRRC26* was highly expressed, as determined by qPCR (Fig. 3A), and it was found that *LRRC26* silencing did not affect cell proliferation (Fig. 3A), consistent with the findings of a previous study using LNCaP prostate cancer cells (18). Next, to further assess the tumor suppressive function of *LRRC26* on the development and progression of TNBC cells, soft agar colony formation, invasion and migration assays were performed to evaluate metastatic properties. Knocking down *LRRC26* expression significantly increased the number of colonies in the soft agar (Fig. 3B), suggesting a critical role for *LRRC26* in anchorage-independent growth. Subsequent Matrigel invasion and migration assays also revealed that siRNA-mediated depletion of *LRRC26* expression led to significant facilitation of HCC70 cell invasion and migration compared with that in siEGFP-transfected cells (Fig. 3C and D). Furthermore, the effects of *LRRC26* overexpression on migration, invasion and cell proliferation in BT-20 cells, which express *LRRC26* at a low level, were examined. The results showed that *LRRC26* overexpression led to a reduction in the migration and invasion and abilities (Fig. 3F and G) of the cells, but did not effect cell viability (Fig. 3H). Taken together, these findings strongly suggest that *LRRC26* suppresses the aggressive behavior of TNBC cells.

LRRC26 expression negatively regulates the TNF-α-induced NF-κB pathway. *LRRC26* has been reported to negatively regulate NF-κB signaling in prostate cancer LNCaP cells (18). Therefore, the effect of *LRRC26* on NF-κB activity was examined in the present study using a luciferase reporter assay and qPCR analysis. A significant time-dependent decrease in luciferase activity was observed in the presence of TNF-α stimulation with ectopic *LRRC26* expression compared with that in the mock control vector in 293T cells (Fig. 4A). qPCR analysis showed that siRNA-mediated *LRRC26*-knockdown significantly increased the TNF-α-induced expression of the NF-κB target genes *IL-6*, *IL-8* and *CXCL1* in HCC70 cells (Fig. 4B). These results suggested that *LRRC26* negatively regulates TNF-α-induced NF-κB activity.

Functional gene annotation clustering analysis. To further clarify the biological role of *LRRC26* in the progression or development of TNBC cells, the present study attempted to identify the processes or pathways associated with *LRRC26* in TNBC cells. siLRRC26, or siEGFP as a control, was transfected into HCC70 cells, which highly express *LRRC26*, and alterations in gene expression were measured using DNA microarray analysis. To identify genes associated with *LRRC26*, genes were selected using the following criterion: Expression level was decreased or increased by >3-fold in siLRRC26-transfected cells compared with that in siEGFP-transfected cells. This approach identified 230 genes that were altered upon *LRRC26*-knockdown (Table V). Among them, the downregulation of olfactory receptor family 5 subfamily M member 1 (*OR5M1*) and *OR5T1* genes, which encode members of olfactory GPCR protein, was verified in *LRRC26*-depleted cells, as determined by qPCR (Fig. 5A). Notably, OR5T1 protein is predicted to be N-glycosylated at Asn17, suggesting the possibility that LRRC26 downregulation may be important for ORT51 glycosylation. To further identify significantly overrepresented Gene Ontology terms affected by *LRRC26* expression in HCC70 cells, these upregulated or downregulated genes were analyzed using the DAVID algorithm (27,31). The most prominent cluster (annotation cluster 1; gene enrichment score, 3.12) was identified, which contained features related to 'glycoprotein', 'signal peptide', 'secreted' and 'N-linked glycoprotein (GlcNAc)' (Table VI). Furthermore, the immunocytochemical staining experiments showed that exogenous HA-LRRC26 was found to be partially co-localized with endogenous GRP78, a molecular chaperone localized in the endoplasmic reticulum (Fig. 5B), and exogenous FLAG-tagged BAP31, an integral membrane protein of the endoplasmic reticulum, in BT20 cells (Fig. 5C), indicating the possibility that LRRC26 may function in the endoplasmic reticulum of TNBC cells. These findings suggested the possibility that *LRRC26* downregulation may affect the secretory pathway from the Golgi apparatus to the cell surface or vesicle transport from the endoplasmic reticulum to the Golgi apparatus in TNBC cells.

Discussion

Genetic and epigenetic inactivation involving DNA methylation and histone modifications of tumor suppressor genes serve a crucial role in the progression and development of breast cancer (20,32). Notably, aberrant promoter hypermethylation of tumor suppressor genes is commonly observed in breast cancer and is the predominant mechanism for loss of function. In the present study, it was demonstrated that *LRRC26* downregulation contributes to the progression and development of TNBC, although further analysis of understanding of the mechanism of *LRRC26* upregulation in breast cancer, particularly ER- and HER2-positive breast cancer, will be necessary.

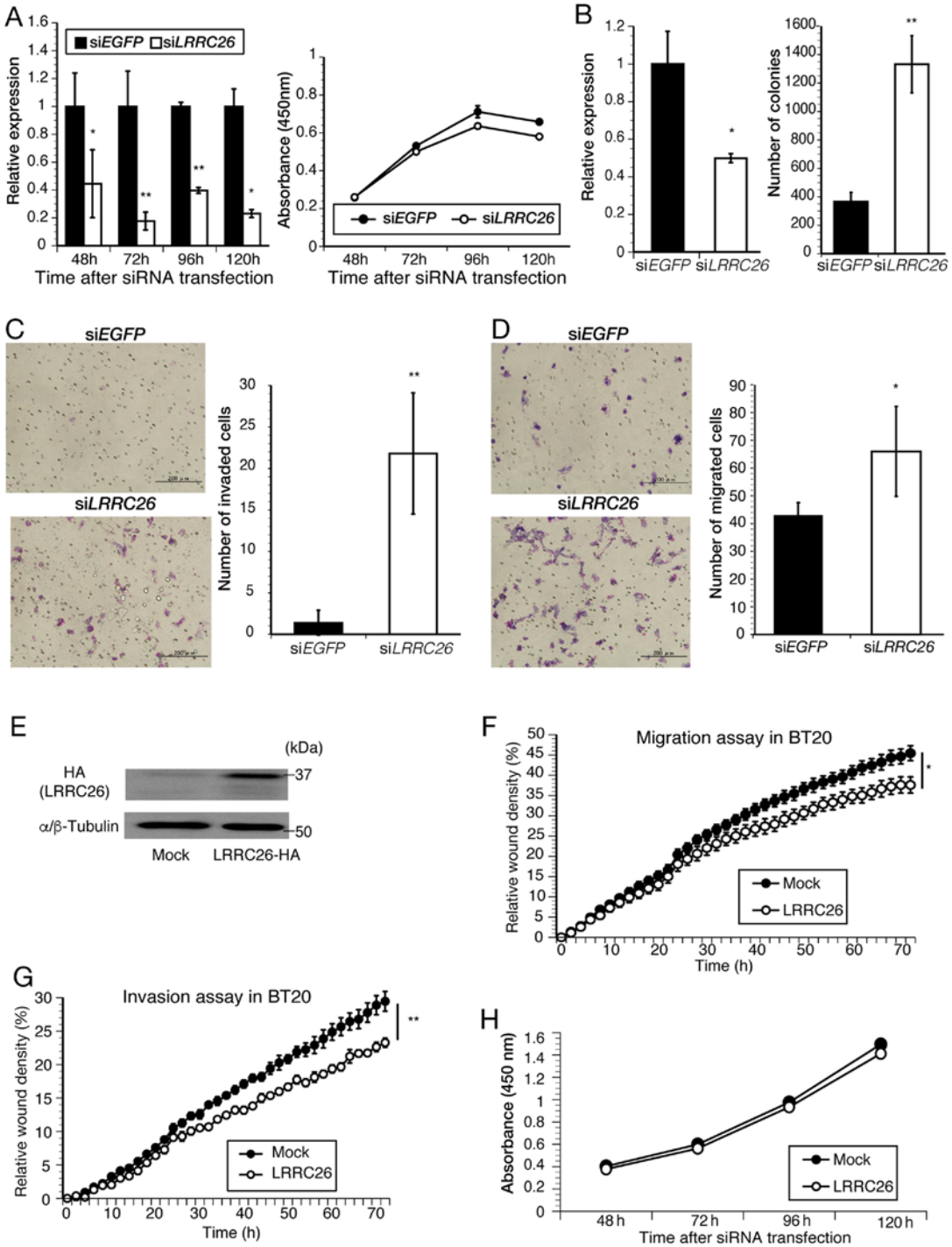

Figure 3. Functional analysis of LRRC26 in HCC70 triple-negative breast cancer cells. (A) qPCR analysis of *LRRC26* in HCC70 cells transfected with siLRRC26 (ON-TARGETplus siRNA) and siEGFP as a control for 48, 72, 96 and 120 h (left panel). (A) Cell proliferation assay was performed to evaluate the growth suppressing effect of *LRRC26* in HCC70 cells (right panel). (B) Soft agar colony formation assays were performed for 36 h to evaluate anchorage-independent growth of *LRRC26* in HCC70 cells (right panel) 11 days after siLRRC26 treatment. qPCR analysis was performed for *LRRC26* in HCC70 cells transfected with siLRRC26 (ON-TARGETplus siRNA) and siEGFP as a control for 36 h (left panel). (C) Cell invasion assay with HCC70 using BD Falcon Cell Culture Inserts at 48 h after siLRRC26 treatment for 36 h. Representative images of invasion assays are shown (left panel). (D) Cell migration assay with HCC70 using Corning Matrigel Invasion Chambers at 48 h after siLRRC26 treatment for 36 h. Representative images of migration assays are shown (left panel). The data represent the mean ± standard deviation of each condition (*P<0.05 and **P<0.01; two-sided Student's t-test). (E) Immunoblotting analysis of LRRC26-HA expression in BT20 cells transfected with LRRC26-HA and an empty vector (Mock) as a control for 48 h. (F) Cell migration of BT20 cells transfected with LRRC26-HA or an empty vector (Mock) were measured using the Incucyte for 72 h after 48 h of transfection. (G) Cell invasion of BT20 cells transfected with LRRC26-HA or an empty vector (Mock) were measured using Incucyte for 72 h after 48 h of transfection. (H) An MTT assay was performed to evaluate the growth suppressing effect of *LRRC26* overexpression in BT20 cells. *LRRC26*, leucine-rich repeat-containing 26; siEGFP, small interfering enhanced green fluorescent protein; qPCR, quantitative polymerase chain reaction.

Although RNA-seq and public TCGA database analyses identified no somatic mutations of the *LRRC26* mRNA in the TNBC tissues and cell lines, the frequent downregulation of *LRRC26* due to promoter hypermethylation at Seq.1 and Seq.2

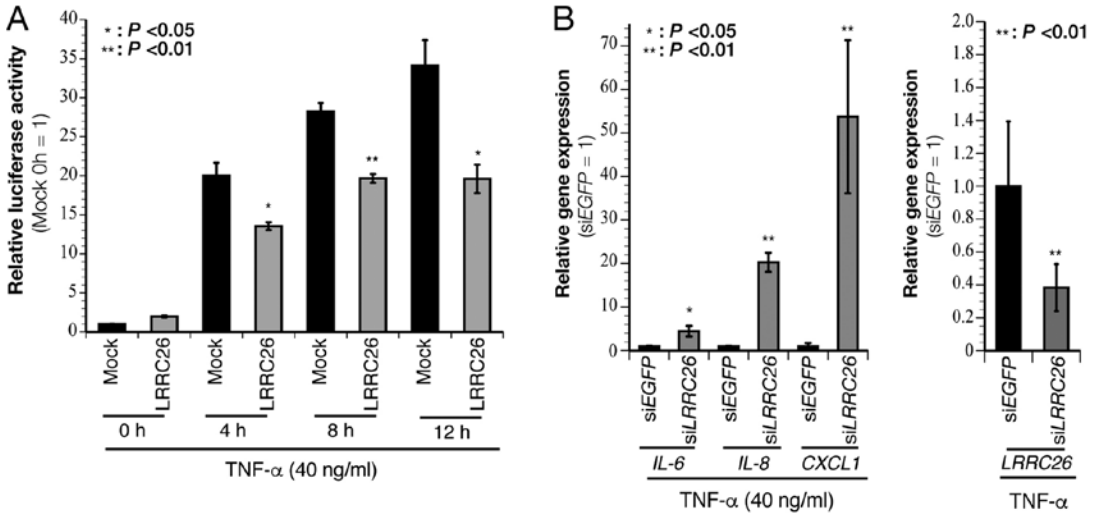

Figure 4. *LRRC26* negatively regulates the NF-κB pathway. (A) Luciferase assay using lysates of 293T cells co-transfected with a luciferase reporter plasmid for NF-κB and a LRRC26 gene plasmid following stimulation with TNF-α (40 ng/ml) for 0, 4, 8 and 12 h, respectively. (B) Quantitative polymerase chain reaction analysis to evaluate the expression of NF-κB-target genes, including *IL-6*, *IL-8* and *CXCL1*, following TNF-α (40 ng/ml) stimulation in siLRRC26-transfected HCC70 cells. The data represent the mean ± standard deviation of each condition (n=3, *P<0.05 and **P<0.01; two-sided Student's t-test). *LRRC26*, leucine-rich repeat-containing 26; EGFP, enhanced green fluorescent protein; NF-κB, nuclear factor-κB; si, small interfering; IL, interleukin; CXCL1, C-X-C motif chemokine ligand-1; TNF-α, tumor necrosis factor-α.

in TNBC tissues and cell lines was observed (Fig. 1B-E). Notably, *LRRC26* was highly expressed in HCC70 cells, but not in MDA-MB-231 cells, whereas *LRRC26* methylation levels at the two CpG sites were similar between HCC70 and MDA-MB-231 cells (Fig. 1D and E). This discrepancy implies the existence of other critical CpG sites in the *LRRC26* promoter region that may be responsible for gene silencing. In fact, the methylation level of the seqTCGA CpG island, located 373 bp upstream of the transcriptional start site, was significantly higher in all tumor tissues compared with that in adjacent normal mammary gland tissues (Fig. 2E). By contrast, *LRRC26* was also not methylated in other CpG islands within 200 bp of the transcription initiation site, particularly around the transcription initiation site of the *LRRC26* gene in HCC70 cells. Notably, miRDB, an online database for miRNA target prediction (33), predicted *LRRC26* as a target of hsa-miR-1275. hsa-miR-1275 is reported to be upregulated in young women (<35 years old) with breast cancer compared with that in older women (>65 and 45-65 years old) (34), as well as in MDA-MB-231 TNBC cells (35), suggesting the possibility that epigenetic and miRNA-mediated inactivation may contribute to *LRRC26* downregulation.

By analyzing TCGA RNA-seq public databases in the present study, it was found that *LRRC26* gene expression was significantly lower in TNBC cases than in ER-positive/HER2-negative and ER-negative/HER2-positive breast cancer cases (Fig. 2C and D), suggesting that hypermethylation-mediated *LRRC26* inactivation may be a TNBC-specific event in the progression and development of cancer cells. Further statistical analysis demonstrated that *LRRC26* downregulation was significantly associated with increased histological grade in patients with TNBC (P=0.017; χ^2 test) (Table IV), whereas Kaplan-Meier analysis revealed no significant association between *LRRC26* downregulation and the overall survival of patients with TNBC (data not shown). These findings suggested that *LRRC26* downregulation may be involved in the aggressiveness of TNBC, but that in addition to *LRRC26* downregulation, other factors may also be necessary to drive malignacy. Further analysis of the association between *LRRC26* downregulation and prognosis using a large number of TNBC samples will also be necessary. Furthermore, *LRRC26* has been reported to suppress tumor growth by negatively regulating NF-κB signaling in LNCaP and MDA-MB-231 cells (18). However, in the present study, the upregulation of NF-κB-target genes in the absence of TNF-α stimulation was not observed in *LRRC26*-depleted HCC70 cells (data not shown), although the upregulation of NF-κB-target genes in the presence of TNF-α stimulation was observed in these cells (Fig. 4B). These results suggest that *LRRC26* downregulation may be important for TNF-α-mediated NF-κB activation in TNBC cells. Furthermore, *LRRC26* expression has been reported to promote anchorage-independent growth in MDA-MB231 cells (18). The present study also found that knocking down *LRRC26* increased not only anchorage-independent growth, but also invasion and migration in HCC70 cells; however, it did not promote proliferation in the absence of TNF-α stimulation, suggesting that *LRRC26* downregulation is critical for the TNF-α-mediated NF-κB-independent progression of TNBC.

To investigate biological roles of *LRRC26* distinct from the NF-κB pathway in TNBC cells, DNA microarray analysis was performed using siLRRC26-transfected HCC70 cells. Functional annotation clustering revealed that upregulated and downregulated genes in *LRRC26*-depleted HCC70 cells are functionally associated with protein secretion and N-linked glycosylation. These findings suggest the possibility that *LRRC26* downregulation may affect the secretory pathway from the Golgi apparatus to the cell surface or vesicle transport from the endoplasmic reticulum to the Golgi apparatus.

LRRC26 protein, a member of the LRR superfamily, has been reported to act as a big potassium (BK) channel auxiliary subunit, whereas the regulation of NF-κB activation

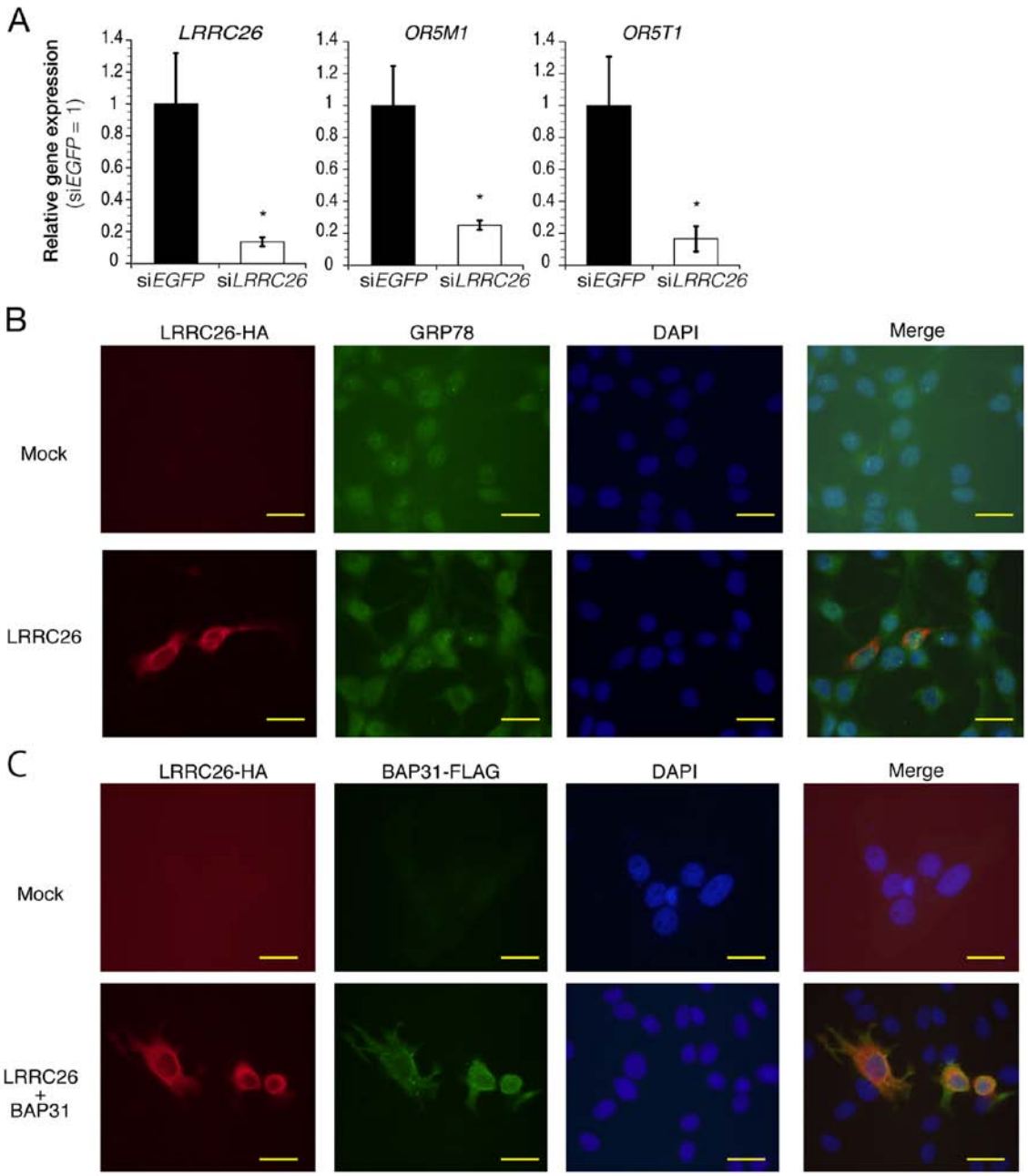

Figure 5. LRRC26 potentially functions in the endoplasmic reticulum in TNBC cells. (A) Verification of downregulation of *OR5M1* and *OR5T1* in LRRC26-depleted cells by quantitative polymerase chain reaction. (B) Exogenous LRRC26-HA was partially merged with endogenous GRP78 in the endoplasmic reticulum of BT20 cells, and immunostained with anti-HA (red) or anti-GRP78 (green) antibodies, and DAPI (blue) to discriminate the nucleus. (C) Co-localization of exogenous LRRC26-HA and BAP31-FLAG in the endoplasmic reticulum of BT20 cells, and immunostained with anti-HA (red) or anti-FLAG (green) antibodies, and DAPI (blue) to discriminate the nucleus. *LRRC26*, leucine-rich repeat-containing 26; *OR5M1*, olfactory receptor family 5 subfamily M member 1; si, small interfering; EGFP, enhanced green fluorescent protein; BAP31, B cell receptor associated protein 31.

by LRRC26 is independent of BK channels (36). Notably, LRRC26 is also predicted to be present on the endoplasmic reticulum membrane via its N-terminal LRR domain, as LRRC26 is N-glycosylated at an Asn147 site in the endoplasmic reticulum (36). LRRC26 has been reported to localize in the endoplasmic reticulum (36). In fact, the present study demonstrated that LRRC26 was observed to be co-localized with GRP78 and BAP31 in the endoplasmic reticulum of TNBC cells (Fig. 5B and C). Moreover, N-linked glycoproteins are composed of a polypeptide glycosylated in the endoplasmic reticulum with several carbonate chains via asparagine residues, and have critical roles in cell-cell interaction and cell adhesion for invasive and metastatic behaviors in breast cancer. These results strongly suggest that *LRRC26* may serve a role in breast cancer progression (37-40). However, further analyses are required to elucidate the effects of *LRRC26* downregulation on N-linked glycosylation in TNBC cells.

In summary, the present study demonstrated that the methylation-mediated inactivation of *LRRC26* resulted in enhancement of anchorage-independent growth-, invasion- and migration-associated metastatic behavior. Notably, frequent methylation-mediated inactivation of *LRRC26* is a TNBC-specific event that may be a potential diagnostic biomarker.

Table V. Genes that were altered upon leucine-rich repeat-containing 26-knockdown according to DNA microarray analysis (n=230).

Gene symbol	Gene name	Fold-change
Upregulation		
ANKRD30A	Ankyrin repeat domain 30A	30.29
MEPE	Matrix extracellular phosphoglycoprotein	26.45
DACT1	Dishevelled-binding antagonist of β-catenin 1	24.11
MGAT5B	Mannosyl (α-1,6-)-glycoprotein β-1,6-N-acetyl-glucosaminyltransferase, isozyme B	17.55
PLCB4	Phospholipase C, β4	17.10
NME8	NME/NM23 family member 8	14.79
HMCN2	Hemicentin 2	13.61
SLC2A7	Solute carrier family 2 (facilitated glucose transporter), member 7	13.57
TSPAN11	Tetraspanin 11	11.90
ACTG2	Actin, gamma 2, smooth muscle, enteric	11.76
CCL11	Chemokine (C-C motif) ligand 11	11.26
GCNT3	Glucosaminyl (N-acetyl) transferase 3, mucin type	10.82
CCDC162P	Coiled-coil domain containing 162, pseudogene	9.65
EWSAT1	Ewing sarcoma associated transcript 1	9.18
DPEP1	Dipeptidase 1 (renal)	9.01
CAMP	Cathelicidin antimicrobial peptide	8.96
PPP1R42	Protein phosphatase 1, regulatory subunit 42	8.01
COL24A1	Collagen, type XXIV, α1	7.82
SCN5A	Sodium channel, voltage gated, type Vα subunit	7.50
TMEM236	Transmembrane protein 236	7.46
ELF5	E74-like factor 5 (ets domain transcription factor)	7.23
ITIH5	Inter-α-trypsin inhibitor heavy chain family, member 5	6.97
NAT2	N-acetyltransferase 2 (arylamine N-acetyltransferase)	6.73
DOCK2	Dedicator of cytokinesis 2	6.45
CFAP61	Cilia and flagella-associated protein 61	6.10
TRPA1	Transient receptor potential cation channel, subfamily A, member 1	6.07
AZU1	Azurocidin 1	5.84
CLNK	Cytokine-dependent hematopoietic cell linker	5.83
MORN3	MORN repeat containing 3	5.58
ARSE	Arylsulfatase E (chondrodysplasia punctata 1)	5.46
FENDRR	FOXF1 adjacent non-coding developmental regulatory RNA	5.27
IZUMO4	IZUMO family member 4	5.09
PHOX2B	Paired-like homeobox 2b	4.99
DKFZP434L187	Uncharacterized LOC26082	4.90
WHAMMP3	WAS protein homolog associated with actin, golgi membranes and microtubules pseudogene 3	4.84
PHYHIP	Phytanoyl-CoA 2-hydroxylase interacting protein	4.81
GRIK2	Glutamate receptor, ionotropic, kainate 2	4.68
CNOT2	CCR4-NOT transcription complex, subunit 2	4.59
CCDC162P	Coiled-coil domain containing 162, pseudogene	4.53
TMEM236	Transmembrane protein 236	4.50
MEGF11	Multiple EGF-like-domains 11	4.44
TMEM35	Transmembrane protein 35	4.39
LDLRAD1	Low density lipoprotein receptor class A domain-containing 1	4.38
FRMD3	FERM domain containing 3	4.34
FGG	Fibrinogen γ chain	4.29
GP6	Glycoprotein VI (platelet)	4.28
C7orf69	Chromosome 7 open reading frame 69	4.21
RNF17	Ring finger protein 17	4.20
PECAM1	Platelet/endothelial cell adhesion molecule 1	4.19

Table V. Continued.

Gene symbol	Gene name	Fold-change
GRIK2	Glutamate receptor, ionotropic, kainate 2	4.16
OR10V1	Olfactory receptor, family 10, subfamily V, member 1	4.11
ASPDH	Aspartate dehydrogenase domain containing	4.02
BCAS1	Breast carcinoma amplified sequence 1	3.99
ANKRD22	Ankyrin repeat domain 22	3.97
ALKBH3-AS1	ALKBH3 antisense RNA 1	3.96
TMEM215	Transmembrane protein 215	3.92
CDSN	Corneodesmosin	3.82
PRR30	Proline rich 30	3.75
CCDC8	Coiled-coil domain-containing 8	3.75
GRAMD1B	GRAM domain-containing 1B	3.70
ANKRD20A12P	Ankyrin repeat domain 20 family, member A12, pseudogene	3.68
OR5D18	Olfactory receptor, family 5, subfamily D, member 18	3.59
FAM209B	Family with sequence similarity 209, member B	3.57
CLEC1B	C-type lectin domain family 1, member B	3.55
USP17L8	Ubiquitin specific peptidase 17-like family member 8	3.54
BMF	Bcl-2 modifying factor	3.52
ZFHX2	Zinc finger homeobox 2	3.52
RBPMS	RNA binding protein with multiple splicing	3.51
TTC29	Tetratricopeptide repeat domain 29	3.49
PCDH11Y	Protocadherin 11 Y-linked	3.48
EFHB	EF-hand domain family, member B	3.44
NBAT1	Neuroblastoma-associated transcript 1	3.41
HEMGN	Hemogen	3.41
WNT3A	Wingless-type MMTV integration site family, member 3A	3.32
PARD6G	Par-6 family cell polarity regulator γ	3.31
KCTD8	Potassium channel tetramerization domain-containing 8	3.30
MGC27382	Uncharacterized MGC27382	3.28
P4HA3	Prolyl 4-hydroxylase, α polypeptide III	3.21
SMIM9	Small integral membrane protein 9	3.19
PTPRC	Protein tyrosine phosphatase, receptor type, C	3.16
KLB	Klotho β	3.13
CLDN19	Claudin 19	3.13
MGC27382	Uncharacterized MGC27382	3.13
ZP1	Zona pellucida glycoprotein 1 (sperm receptor)	3.13
PTPRC	Protein tyrosine phosphatase, receptor type, C	3.12
C15orf32	Chromosome 15 open reading frame 32	3.11
NLRP12	NLR family, pyrin domain containing 12	3.11
POLH	Polymerase (DNA directed), η	3.08
KIAA1731NL	KIAA1731 N-terminal like	3.06
PRPS1	Phosphoribosyl pyrophosphate synthetase 1	3.05
Downregulation		
DCAF12L1	DDB1 and CUL4 associated factor 12-like 1	-31.73
REG3A	Regenerating islet-derived 3 α	-29.34
CXorf21	Chromosome X open reading frame 21	-23.23
TAT	Tyrosine aminotransferase	-22.82
MS4A12	Membrane-spanning 4-domains, subfamily A, member 12	-22.56
OR5M1	Olfactory receptor, family 5, subfamily M, member 1	-20.76
C10orf90	Chromosome 10 open reading frame 90	-19.70
ADAM5	ADAM metallopeptidase domain 5 (pseudogene)	-18.73
HNRNPKP3	Heterogeneous nuclear ribonucleoprotein K pseudogene 3	-17.57
BMP7	Bone morphogenetic protein 7	-17.32

Table V. Continued.

Gene symbol	Gene name	Fold-change
OR5T1	Olfactory receptor, family 5, subfamily T, member 1	-16.91
AQP10	Aquaporin 10	-16.63
NBAT1	Neuroblastoma associated transcript 1	-16.43
OR1A1	Olfactory receptor, family 1, subfamily A, member 1	-16.24
CALY	Calcyon neuron-specific vesicular protein	-15.47
MAP3K13	Mitogen-activated protein kinase kinase kinase 13	-14.49
NCRNA00249	Uncharacterized LOC101926947	-13.95
SLC22A11	Solute carrier family 22 (organic anion/urate transporter), member 11	-13.81
SNORD116-11	Small nucleolar RNA, C/D box 116-11	-13.67
LILRB4	Leukocyte immunoglobulin-like receptor, subfamily B (with TM and ITIM domains), member 4	-13.62
ERVV-2	Endogenous retrovirus group V, member 2	-13.31
TTC24	Tetratricopeptide repeat domain 24	-12.83
PCDHB15	Protocadherin β15	-11.64
ZNF705G	Zinc finger protein 705G	-10.80
FAM20A	Family with sequence similarity 20, member A	-10.79
LILRA3	Leukocyte immunoglobulin-like receptor, subfamily A (without TM domain), member 3	-10.65
PALM2	Paralemmin 2	-10.33
RSPH6A	Radial spoke head 6 homolog A (*Chlamydomonas*)	-10.25
ANGPTL1	Angiopoietin-like 1	-10.14
ATP8B2	ATPase, aminophospholipid transporter, class I, type 8B, member 2	-10.07
FMO9P	Flavin containing monooxygenase 9 pseudogene	-9.60
MEIS1-AS2	MEIS1 antisense RNA 2	-9.47
PKDCC	Protein kinase domain containing, cytoplasmic	-9.20
RBMY1B	RNA binding motif protein, Y-linked, family 1, member B	-9.19
CFAP46	Cilia and flagella-associated protein 46	-9.06
BIRC8	Baculoviral IAP repeat-containing 8	-8.96
PENK	Proenkephalin	-8.95
C9orf47	Chromosome 9 open reading frame 47	-8.73
PRDM16	PR domain containing 16	-8.70
FAM104B	Family with sequence similarity 104, member B	-8.54
NLRP4	NLR family, pyrin domain containing 4	-8.51
MOV10L1	Mov10 RISC complex RNA helicase like 1	-8.30
SLAMF8	SLAM family member 8	-8.28
C7orf71	Chromosome 7 open reading frame 71	-8.18
SOGA3	SOGA family member 3	-8.16
SLC2A1-AS1	SLC2A1 antisense RNA 1	-8.15
TXNDC8	Thioredoxin domain-containing 8 (spermatozoa)	-7.80
PCLO	Piccolo presynaptic cytomatrix protein	-7.75
RNF17	Ring finger protein 17	-7.69
ACADL	Acyl-CoA dehydrogenase, long chain	-7.46
GPR123	G protein-coupled receptor 123	-7.41
RPS6KA2-AS1	RPS6KA2 antisense RNA 1	-7.26
LRRC34	Leucine rich repeat containing 34	-7.21
TMEM98	Transmembrane protein 98	-7.18
DACT2	Dishevelled-binding antagonist of β-catenin 2	-6.94
C20orf173	Chromosome 20 open reading frame 173	-6.85
TBX18	T-box 18	-6.64
ANKRD62	Ankyrin repeat domain 62	-6.43
VAX1	Ventral anterior homeobox 1	-6.15
PIP5K1B	Phosphatidylinositol-4-phosphate 5-kinase, type I, β	-6.07
MZB1	Marginal zone B and B1 cell-specific protein	-6.04

Table V. Continued.

Gene symbol	Gene name	Fold-change
MIR3663HG	miR3663 host gene (non-protein coding)	-6.03
DEFB133	Defensin, β133	-5.99
MMP13	Matrix metallopeptidase 13 (collagenase 3)	-5.94
ZFYVE28	Zinc finger, FYVE domain containing 28	-5.82
DUX3	Double homeobox 3	-5.81
IFNL3	Interferon λ3	-5.80
MT1DP	Metallothionein 1D, pseudogene (functional)	-5.61
TP53AIP1	Tumor protein p53 regulated apoptosis inducing protein 1	-5.50
KCNMA1	Potassium channel, calcium activated large conductance subfamily Mα, member 1	-5.47
MRPL23-AS1	MRPL23 antisense RNA 1	-5.41
PCSK1	Proprotein convertase subtilisin/kexin type 1	-5.37
IPW	Imprinted in Prader-Willi syndrome (non-protein coding)	-5.24
UPK1A	Uroplakin 1A	-5.09
NAIP	NLR family, apoptosis inhibitory protein	-4.84
ABI3BP	ABI family, member 3 (NESH) binding protein	-4.79
ENDOV	Endonuclease V	-4.66
MAP2	Microtubule-associated protein 2	-4.66
HMBOX1	Homeobox containing 1	-4.65
CHIAP2	Chitinase, acidic pseudogene 2	-4.60
BMS1P17	BMS1 pseudogene 17	-4.52
SPOCK3	Sparc/osteonectin, cwcv and kazal-like domains proteoglycan (testican) 3	-4.51
RASSF3	Ras association (RalGDS/AF-6) domain family member 3	-4.51
SLC24A1	Solute carrier family 24 (sodium/potassium/calcium exchanger), member 1	-4.47
NR1H2	Nuclear receptor subfamily 1, group H, member 2	-4.46
RBMY1B	RNA binding motif protein, Y-linked, family 1, member B	-4.42
BPIFB4	BPI fold containing family B, member 4	-4.39
RAG2	Recombination activating gene 2	-4.34
RBMXL2	RNA binding motif protein, X-linked-like 2	-4.26
MASP1	Mannan-binding lectin serine peptidase 1 (C4/C2 activating component of Ra-reactive factor)	-4.25
AIPL1	Aryl hydrocarbon receptor interacting protein-like 1	-4.16
SGPP2	Sphingosine-1-phosphate phosphatase 2	-4.13
PLGLB1	Plasminogen-like B1	-4.12
NPAS3	Neuronal PAS domain protein 3	-4.09
FLJ16734	Uncharacterized LOC641928	-4.06
LRRTM4	Leucine rich repeat transmembrane neuronal 4	-4.04
TPTE2	Transmembrane phosphoinositide 3-phosphatase and tensin homolog 2	-3.95
FLJ36777	Uncharacterized LOC730971	-3.91
DNAI1	Dynein, axonemal, intermediate chain 1	-3.88
ROBO4	Roundabout, axon guidance receptor, homolog 4 (*Drosophila*)	-3.84
ALOX15	Arachidonate 15-lipoxygenase	-3.79
OLIG3	Oligodendrocyte transcription factor 3	-3.78
MON2	MON2 homolog (*S. cerevisiae*)	-3.76
MON2	MON2 homolog (*S. cerevisiae*)	-3.75
CASC11	Cancer susceptibility candidate 11 (non-protein coding)	-3.68
CRISP2	Cysteine-rich secretory protein 2	-3.68
RAB41	RAB41, member RAS oncogene family	-3.61
ALS2CR12	Amyotrophic lateral sclerosis 2 (juvenile) chromosome region, candidate 12	-3.56
GLYCTK	Glycerate kinase	-3.55
NCRNA00250	Non-protein coding RNA 250	-3.51
VCAM1	Vascular cell adhesion molecule 1	-3.44
OPALIN	Oligodendrocytic myelin paranodal and inner loop protein	-3.41
AKNAD1	AKNA domain containing 1	-3.40

Table V. Continued.

Gene symbol	Gene name	Fold-change
ATP1A2	ATPase, Na^+/K^+ transporting, α2 polypeptide	-3.39
OTOGL	Otogelin-like	-3.35
MUC6	Mucin 6, oligomeric mucus/gel-forming	-3.33
FAM230A	Family with sequence similarity 230, member A	-3.32
KRT6A	Keratin 6A, type II	-3.32
SLC25A21-AS1	SLC25A21 antisense RNA 1	-3.31
GLYCTK	Glycerate kinase	-3.29
DRD2	Dopamine receptor D2	-3.29
CECR6	Cat eye syndrome chromosome region, candidate 6	-3.29
PRKCQ-AS1	PRKCQ antisense RNA 1	-3.28
ADAMTS6	ADAM metallopeptidase with thrombospondin type 1 motif, 6	-3.27
CCDC178	Coiled-coil domain containing 178	-3.26
LTN1	Listerin E3 ubiquitin protein ligase 1	-3.25
C10orf71-AS1	C10orf71 antisense RNA 1	-3.23
SPDYE5	Speedy/RINGO cell cycle regulator family member E5	-3.21
CD180	CD180 molecule	-3.20
DPY19L2	Dpy-19-like 2 *(C. elegans)*	-3.20
SCEL	Sciellin	-3.13
PTGIR	Prostaglandin I2 (prostacyclin) receptor (IP)	-3.10
ABCB1	ATP-binding cassette, sub-family B (MDR/TAP), member 1	-3.10
ABCC2	ATP-binding cassette, sub-family C (CFTR/MRP), member 2	-3.09
MYL10	Myosin, light chain 10, regulatory	-3.07
OR5M9	Olfactory receptor, family 5, subfamily M, member 9	-3.06
APCDD1L-AS1	APCDD1L antisense RNA 1 (head to head)	-3.06
SULT1B1	Sulfotransferase family, cytosolic, 1B, member 1	-3.05
CFAP58	Cilia and flagella-associated protein 58	-3.03
TERF1	Telomeric repeat binding factor (NIMA-interacting) 1	-3.03

Table VI. Functional gene annotation clustering analysis of annotation cluster one (enrichment score: 3.12) based on the Database for Annotation, Visualization and Integrated Discovery algorithm[a].

Category	Term	No. of genes	P-value
UP_KEYWORDS	Glycoprotein	66	$8.32x10^{-5}$
UP_SEQ_FEATURE	Signal peptide	51	$1.21x10^{-4}$
UP_SEQ_FEATURE	Glycosylation site:N-linked (GlcNAc...)	58	$5.77x10^{-4}$
UP_KEYWORDS	Secreted	33	$1.09x10^{-3}$
UP_KEYWORDS	Signal	57	$1.45x10^{-3}$
UP_KEYWORDS	Disulfide bond	49	$1.64x10^{-3}$

[a]Partial list of a functional annotation cluster was obtained by loading 216 genes, the expression of which included an increase or decrease of >3-fold following knockdown of leucine-rich repeat-containing 26 in HCC70 cells using a DNA microarray analysis.

Acknowledgements

The authors would like to thank Dr Junichi Kurebayashi (Kawasaki Medical School, Kurashiki, Okayama, Japan) for gifting the KPL-3C breast cancer cell line, and Ms. Hinako Koseki and Ms. Hitomi Kawakami (Division of Genome Medicine, Institute for Genome Research, Tokushima University, Tokushima, Japan) for providing excellent technical support.

Funding

This research was supported by the Tailor-Made Medical Treatment with the BBJ Project (grant no. 13418656) and Practical Research for Innovative Cancer Control (grant no. 12103129) from the Japan Agency for Medical Research and Development.

Availability of data and materials

The assessed TCGA data set was from the TCGA portal (http://cancergenome.nih.gov/). The RNA-Seq data (accession no. JGAS00000000116) used in Fig. 1A were deposit

in the DNA DataBank of Japan (http://www.ddbj.nig.ac.jp/). The microarray data (GSE90582) were submitted to the NCBI Gene Expression Omnibus archive (https://www.ncbi.nlm.nih.gov/geo/).

Authors' contributions

YMiyagawa performed all experiments, interpreted all data and prepared the draft of the manuscript. YMatsushita performed the analyses for *LRRC26* expression, invasion, migration assay by Incucyte and immunocytochemical staining, interpreted all data and prepared the draft and final version of the manuscript. HS performed the methylation of *LRRC26* and analyses for TCGA data sets. MK and TY provided the interpretation of *LRRC26* expression and function. RK performed the analyses for the luciferase assay. AY and AT provided the interpretation of the clinical association data. JH and MS prepared the clinical specimens and provided the interpretation of the clinical association data. YMiyoshi discussed the interpretation of all data. TK was involved in the conception and design of all studies, the interpretation of the data, and the preparation of the draft and final version of the manuscript. All authors read and approved the final manuscript.

Ethics approval and consent to participate

The present study, as well as the use of all clinical materials aforementioned, was approved by the Ethics Committee of Tokushima University (permission no. H29-15 for expression profile analysis and permission no. H29-14 for RNA-seq analysis).

Consent for publication

Clinical specimens were obtained with informed consent from patients who were treated at the Tokushima Breast Care Clinic (Tokushima, Japan), as previously described (20), with permission to publish their data.

Competing interests

The authors declare that they have no competing interests.

References

1. Fisher B, Anderson S, Tan-Chiu E, Wolmark N, Wickerham DL, Fisher ER, Dimitrov NV, Atkins JN, Abramson N, Merajver S, *et al*: Tamoxifen and chemotherapy for axillary node-negative, estrogen receptor-negative breast cancer: Findings from National Surgical Adjuvant Breast and Bowel Project B-23. J Clin Oncol 19: 931-942, 2001.
2. Colleoni M, Gelber S, Goldhirsch A, Aebi S, Castiglione-Gertsch M, Price KN, Coates AS and Gelber RD; International Breast Cancer Study Group: Tamoxifen after adjuvant chemotherapy for premenopausal women with lymph node-positive breast cancer: International Breast Cancer Study Group Trial 13-93. J Clin Oncol 24: 1332-1341, 2006.
3. Merglen A, Verkooijen HM, Fioretta G, Neyroud-Caspar I, Vinh-Hung V, Vlastos G, Chappuis PO, Castiglione M, Rapiti E and Bouchardy C: Hormonal therapy for oestrogen receptor-negative breast cancer is associated with higher disease-specific mortality. Ann Oncol 20: 857-861, 2009.
4. Huszno J and Nowara E: Current therapeutic strategies of anti-HER2 treatment in advanced breast cancer patients. Contemp Oncol (Pozn) 20: 1-7, 2016.
5. Foulkes WD, Smith IE and Reis-Filho JS: Triple-negative breast cancer. N Engl J Med 363: 1938-1948, 2010.
6. Liedtke C, Mazouni C, Hess KR, André F, Tordai A, Mejia JA, Symmans WF, Gonzalez-Angulo AM, Hennessy B, Green M, *et al*: Response to neoadjuvant therapy and long-term survival in patients with triple-negative breast cancer. J Clin Oncol 26: 1275-1281, 2008.
7. Gradishar WJ, Anderson BO, Balassanian R, Blair SL, Burstein HJ, Cyr A, Elias AD, Farrar WB, Forero A, Giordano SH, *et al*: Invasive Breast Cancer Version 1.2016, NCCN Clinical Practice Guidelines in Oncology. J Natl Compr Canc Netw 14: 324-354, 2016.
8. Cortes J, O'Shaughnessy J, Loesch D, Blum JL, Vahdat LT, Petrakova K, Chollet P, Manikas A, Diéras V, Delozier T, *et al*; EMBRACE (Eisai Metastatic Breast Cancer Study Assessing Physician's Choice Versus E7389) investigators: Eribulin monotherapy versus treatment of physician's choice in patients with metastatic breast cancer (EMBRACE): A phase 3 open-label randomised study. Lancet 377: 914-923, 2011.
9. Denkert C, Liedtke C, Tutt A and von Minckwitz G: Molecular alterations in triple-negative breast cancer-the road to new treatment strategies. Lancet 389: 2430-2442, 2017.
10. Kim JE, Ahn HJ, Ahn JH, Yoon DH, Kim SB, Jung KH, Gong GY, Kim MJ, Son BH and Ahn SH: Impact of triple-negative breast cancer phenotype on prognosis in patients with stage I breast cancer. J Breast Cancer 15: 197-202, 2012.
11. Lehmann BD, Bauer JA, Chen X, Sanders ME, Chakravarthy AB, Shyr Y and Pietenpol JA: Identification of human triple-negative breast cancer subtypes and preclinical models for selection of targeted therapies. J Clin Invest 121: 2750-2767, 2011.
12. Cancer Genome Atlas N; Cancer Genome Atlas Network: Comprehensive molecular portraits of human breast tumours. Nature 490: 61-70, 2012.
13. Pereira B, Chin SF, Rueda OM, Vollan HK, Provenzano E, Bardwell HA, Pugh M, Jones L, Russell R, Sammut SJ, *et al*: The somatic mutation profiles of 2,433 breast cancers refines their genomic and transcriptomic landscapes. Nat Commun 7: 11479, 2016.
14. Shah SP, Roth A, Goya R, Oloumi A, Ha G, Zhao Y, Turashvili G, Ding J, Tse K, Haffari G, *et al*: The clonal and mutational evolution spectrum of primary triple-negative breast cancers. Nature 486: 395-399, 2012.
15. O'Shaughnessy J, Osborne C, Pippen JE, Yoffe M, Patt D, Rocha C, Koo IC, Sherman BM and Bradley C: Iniparib plus chemotherapy in metastatic triple-negative breast cancer. N Engl J Med 364: 205-214, 2011.
16. Tutt A, Robson M, Garber JE, Domchek SM, Audeh MW, Weitzel JN, Friedlander M, Arun B, Loman N, Schmutzler RK, *et al*: Oral poly(ADP-ribose) polymerase inhibitor olaparib in patients with BRCA1 or BRCA2 mutations and advanced breast cancer: A proof-of-concept trial. Lancet 376: 235-244, 2010.
17. Yamaguchi N, Ito T, Azuma S, Ito E, Honma R, Yanagisawa Y, Nishikawa A, Kawamura M, Imai J, Watanabe S, *et al*: Constitutive activation of nuclear factor-kappaB is preferentially involved in the proliferation of basal-like subtype breast cancer cell lines. Cancer Sci 100: 1668-1674, 2009.
18. Liu XF, Xiang L, Zhang Y, Becker KG, Bera TK and Pastan I: CAPC negatively regulates NF-κB activation and suppresses tumor growth and metastasis. Oncogene 31: 1673-1682, 2012.
19. Kurebayashi J, Kurosumi M and Sonoo H: A new human breast cancer cell line, KPL-3C, secretes parathyroid hormone-related protein and produces tumours associated with microcalcifications in nude mice. Br J Cancer 74: 200-207, 1996.
20. Komatsu M, Yoshimaru T, Matsuo T, Kiyotani K, Miyoshi Y, Tanahashi T, Rokutan K, Yamaguchi R, Saito A, Imoto S, *et al*: Molecular features of triple negative breast cancer cells by genome-wide gene expression profiling analysis. Int J Oncol 42: 478-506, 2013.
21. Livak KJ and Schmittgen TD: Analysis of relative gene expression data using real-time quantitative PCR and the 2(-Delta Delta C(T)) method. Methods 25: 402-408, 2001.
22. Kim JW, Akiyama M, Park JH, Lin ML, Shimo A, Ueki T, Daigo Y, Tsunoda T, Nishidate T, Nakamura Y, *et al*: Activation of an estrogen/estrogen receptor signaling by BIG3 through its inhibitory effect on nuclear transport of PHB2/REA in breast cancer. Cancer Sci 100: 1468-1478, 2009.
23. Park JH, Lin ML, Nishidate T, Nakamura Y and Katagiri T: PDZ-binding kinase/T-LAK cell-originated protein kinase, a putative cancer/testis antigen with an oncogenic activity in breast cancer. Cancer Res 66: 9186-9195, 2006.

24. Kamimae S, Yamamoto E, Kai M, Niinuma T, Yamano HO, Nojima M, Yoshikawa K, Kimura T, Takagi R, Harada E, *et al*: Epigenetic silencing of NTSR1 is associated with lateral and noninvasive growth of colorectal tumors. Oncotarget 6: 29975-29990, 2015.
25. Ng FW, Nguyen M, Kwan T, Branton PE, Nicholson DW, Cromlish JA and Shore GC: p28 Bap31, a Bcl-2/Bcl-XL- and procaspase-8-associated protein in the endoplasmic reticulum. J Cell Biol 139: 327-338, 1997.
26. Annaert WG, Becker B, Kistner U, Reth M and Jahn R: Export of cellubrevin from the endoplasmic reticulum is controlled by BAP31. J Cell Biol 139: 1397-1410, 1997.
27. Huang W, Sherman BT and Lempicki RA: Systematic and integrative analysis of large gene lists using DAVID bioinformatics resources. Nat Protoc 4: 44-57, 2009.
28. Huang W, Sherman BT and Lempicki RA: Bioinformatics enrichment tools: Paths toward the comprehensive functional analysis of large gene lists. Nucleic Acids Res 37: 1-13, 2009.
29. Hao JM, Chen JZ, Sui HM, Si-Ma XQ, Li GQ, Liu C, Li JL, Ding YQ and Li JM: A five-gene signature as a potential predictor of metastasis and survival in colorectal cancer. J Pathol 220: 475-489, 2010.
30. Yoshimaru T, Komatsu M, Matsuo T, Chen YA, Murakami Y, Mizuguchi K, Mizohata E, Inoue T, Akiyama M, Yamaguchi R, *et al*: Targeting BIG3-PHB2 interaction to overcome tamoxifen resistance in breast cancer cells. Nat Commun 4: 2443, 2013.
31. Kajiura K, Masuda K, Naruto T, Kohmoto T, Watabnabe M, Tsuboi M, Takizawa H, Kondo K, Tangoku A and Imoto I: Frequent silencing of the candidate tumor suppressor TRIM58 by promoter methylation in early-stage lung adenocarcinoma. Oncotarget 8: 2890-2905, 2017.
32. Locke WJ and Clark SJ: Epigenome remodelling in breast cancer: Insights from an early in vitro model of carcinogenesis. Breast Cancer Res 14: 215, 2012.
33. Wang X: miRDB: A microRNA target prediction and functional annotation database with a wiki interface. RNA 14: 1012-1017, 2008.
34. Peña-Chilet M, Martínez MT, Pérez-Fidalgo JA, Peiró-Chova L, Oltra SS, Tormo E, Alonso-Yuste E, Martinez-Delgado B, Eroles P, Climent J, *et al*: MicroRNA profile in very young women with breast cancer. BMC Cancer 14: 529, 2014.
35. Nguyen HT, Li C, Lin Z, Zhuang Y, Flemington EK, Burow ME, Lin YI and Shan B: The microRNA expression associated with morphogenesis of breast cancer cells in three-dimensional organotypic culture. Oncol Rep 28: 117-126, 2012.
36. Yan J and Aldrich RW: BK potassium channel modulation by leucine-rich repeat-containing proteins. Proc Natl Acad Sci USA 109: 7917-7922, 2012.
37. Carvalho S, Oliveira T, Bartels MF, Miyoshi E, Pierce M, Taniguchi N, Carneiro F, Seruca R, Reis CA, Strahl S, *et al*: O-mannosylation and N-glycosylation: Two coordinated mechanisms regulating the tumour suppressor functions of E-cadherin in cancer. Oncotarget 7: 65231-65246, 2016.
38. Couldrey C and Green JE: Metastases: The glycan connection. Breast Cancer Res 2: 321-323, 2000.
39. Dall'Olio F, Malagolini N, Trinchera M and Chiricolo M: Mechanisms of cancer-associated glycosylation changes. Front Biosci (Landmark Ed) 17: 670-699, 2012.
40. Pinho SS and Reis CA: Glycosylation in cancer: Mechanisms and clinical implications. Nat Rev Cancer 15: 540-555, 2015.
41. Wolff AC, Hammond ME, Hicks DG, Dowsett M, McShane LM, Allison KH, Allred DC, Bartlett JM, Bilous M, Fitzgibbons P, *et al*; American Society of Clinical Oncology; College of American Pathologists: Recommendations for human epidermal growth factor receptor 2 testing in breast cancer: American Society of Clinical Oncology/College of American Pathologists clinical practice guideline update. J Clin Oncol 31: 3997-4013, 2013.
42. Sobin L, Gospodarowicz M and Wittekind C (eds): TNM Classification of Malignant Tumors. John Wiley & Sons, Inc., Hoboken, NJ, 2010.